Flow Analysis of Non-Spherical Granular Materials in a Two-Dimensional Hopper

by

Abdolreza Mortezapour

B.Sc., Hormozgan University, Iran, 2008

M.Sc., Tehran I.A.U., Iran, 2011

A Thesis Submitted in Partial Fulfillment of the
Requirements for the Degree of

MASTER OF APPLIED SCIENCE
In the Department of Mechanical Engineering

University of Victoria

Flow Analysis of Non-Spherical Granular Materials in a Two-Dimensional Hopper

by

Abdolreza Mortezapour

B.Sc., Hormozgan University, Iran, 2008

M.Sc., Tehran I.A.U., Iran, 2011

Supervisory Committee

Dr. Ben Nadler, Supervisor

Department of Mechanical Engineering

Dr. Peter Oshkai, Department Member

Department of Mechanical Engineering

Abstract

Non-spherical granular materials have been of an interest for the various research communities and industries due to their widespread presence in natural and engineered systems. These materials, which include substances like soil, powders, dry sludges, and grains, exhibit complex behaviors influenced by factors such as grains interactions and boundary conditions. Under sufficient conditions, these materials can flow, ranking second only to water as the most handled materials in diverse industries. Therefore, understanding how these materials flow is important in different domains, from wastewater treatment and mining to food and pharmaceutical industries.

Granular flow within hoppers, driven by gravity, provides cost-effective transportation and is widely used in material handling and storage systems. This research aims to investigate the behavior of non-spherical grains in flow within a hopper through implementing a Finite Element Analysis (FEA) suite and using a previously developed model for non-spherical granular flow. A simulation similar to an available experiment is conducted by implementing the developed model for both spherical and non-spherical grains. The results from the simulation consistently align with those of the experiment, demonstrating the validity and accuracy of the simulation. Moving forward, more complex conditions in a practical application are examined to showcase the capability of the model and the implementation approach. The simulation results reveal the effect of boundary conditions and model parameters on grains orientation and flow within the hopper.

The main motivation behind this research lies in establishing a foundation for utilizing the capabilities of a FEA suite to facilitate further investigations

spanning a broad range of geometries and conditions, addressing challenges in numerical modeling of complex non-spherical granular flows.

The outcome of this research in successfully integrating the developed model into the suite and simulating granular flow in different conditions and geometries, can be employed for further studies with practical significance for industries dealing with granular materials. It lays the groundwork for implementing a versatile FEA suite to simulate complex behaviors of granular materials. This foundation is viable for further studies addressing potential issues related to grain flow in hoppers, aiming to optimize industrial processes and improve material handling and storage techniques.

Keywords: Granular flow · Non-spherical grains · Orientation · Material handling · Finite Element Analysis implementation · Hopper

Table of Contents

List of Figures

List of Tables

Acknowledgements

I am immensely grateful for the substantial support and assistance I have received during the course of this thesis. I wish to extend my heartfelt appreciation to my supervisor and mentor, Dr. Ben Nadler, whose unwavering guidance, support, and encouragement have proven indispensable throughout the entirety of this research endeavor, not only in this acknowledgment but throughout my entire journey at the University of Victoria.

I would also like to convey my thanks to the members of the supervisory committee for their dedicated time and effort in evaluating and enriching my research.

Additionally, I am indebted to my friend, Meitham Amereh, whose counsel and insightful advice have been invaluable companions on this academic journey.

Finally, I would like to thank my wife, Haniyeh, who supported me spiritually throughout my study.

Dedication

This thesis is dedicated to my father. While I was far from him for an extended period during the completion of this thesis, I experienced the profound loss of my father. I want to convey my deep appreciation for all the love and dedication he showered upon me. May his soul rest in peace. Thank you, Dad.

Chapter 1

1. Introduction

This chapter gives a concise overview of granular materials and their associated flows. It explores the historical context of hydrodynamics models in the field of granular materials, exploring their significance in both industrial applications and the natural world. Furthermore, it outlines the primary goals and impacts of this study.

1.1. Granular Material Definition

Granular materials are a collection of discrete, mesoscopic solid grains. Granular materials consist of grains in contact and surrounding voids [1]. The micromechanical behavior of granular materials is inherently discontinuous. The macroscopic (overall or averaged) behavior of granular materials is determined not only by how discrete grains are arranged in space, but also by what kinds of interactions are operating among them. To understand the mechanical behavior of granular materials from a microscopic point of view, the spatial distribution of grains and their contact and collision conditions should primarily be specified. A diverse range of substances fall under the category of granular materials, including gravels, sand, coal, nuts, rice, coffee, corn, powders, capsules, and bearing balls. Examples of these grains are illustrated in Figure 1.1. These grains cannot be classified within traditional solid, liquid, or gas formations. The material's behavior exhibits a spectrum, transitioning from a solid-like state capable of supporting static shear loads to a liquid-like condition allowing flow in a dense state, and even to a gas-like state wherein grains can separate and collide. Granular materials hold significant commercial importance across multiple sectors, spanning the pharmaceutical industry, agriculture, food processing and energy production [2].

Figure 1.1. Examples of non-spherical granular materials

Under the sufficient conditions, a granular solid can flow. This was probably first recorded by Lucretius (ca. 98–55 B.C.), who wrote, 'One can scoop up poppy seeds with a ladle as easily as if they were water, and when dipping the ladle, the seeds flow in a continuous stream' [3]. As long as there has been mining and agriculture, people have sought to harness the flowability of granular materials to facilitate handling and storage applications. Specifically, the capacity of gravity to propel a granular flow significantly simplifies and offers a cost-efficient means of transport. Consequently, gravity-driven flows are integral to the operation of common granular handling devices, such as hoppers.

In general, the spaces between the grains are filled with an interstitial fluid/gas. However, it will be assumed herein that the grains are large and heavy in the sense that they are insensitive to the effects of the interstitial fluid/gas. Granular materials are considered with no cohesion between grains; cohesion arises from surface forces or related phenomena such as liquid bridges, both of which act on the surface area and thus can generally be neglected for large enough grains with small surface area-to-volume ratios. Note that these requirements collectively define what is meant by 'large', although those criteria cannot yet be quantitatively defined by a set of dimensionless parameters [3].

Granular material with no significant fluids between its grains is referred to as dry granular material [4]. These materials are cohesionless and only carry repulsive contact forces between their components, as illustrated in Figure 1.2. As can be seen

in this figure, when a normal force activated at the contact point, acting perpendicular to the plane tangent to the surface of two grains at that particular point. Since the direction of the force does not necessarily pass through the grains center, a repulsive force supplemented by a torque applied at the center of grains showing the impact of the contact forces on the orientation of the grains [5].

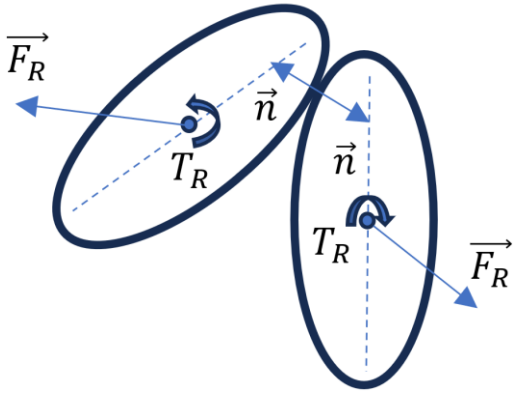

Figure 1.2. Repulsive force between grains

Understanding the conditions under which granular media transition from a solid, jammed state to one that can flow, and the role of orientation is essential for controlling granular flows. In complex scenarios where conducting physical experiments is impractical due to constraints such as time, cost, and resource limitations, the need for continuum models becomes evident for better understanding. However, despite the common presence of granular materials and their diverse applications, the development of continuum models has not yet reached a stage where they can consistently and accurately predict the behavior of non-spherical granular materials during flow [6].

In the following section, a comprehensive review of the existing literature in this field is presented.

1.2. Literature Review

Dense flows, where direct grain-grain interactions play a dominant role, encompass a wide range of areas. These include slurry pipelines [7], granular material storage

[8], fluidized beds [9], mining and milling operations, ploughing [10], abrasive water jet machining, food processing, debris flows [11], avalanches [12], landslides, sediment transport, and earthquake-induced soil liquefaction [13].

Various experimental and computational methods have been developed over time to explore the behavior of granular materials during flow and understand how their mechanical response correlates with their microstructure. However, the creation of a predictive model for the material behavior during flow has the potential to reduce the reliance on extensive physical experiments and complex discrete numerical simulations.

In pursuit of this goal, continuum models have been developed to describe granular materials at a macroscopic level. In this framework, the properties of the continuum system are treated as continuous, ensuring that even when dealing with infinitesimal volumes of material, these properties persist. Over time, different theories developed to different type of grains and flow conditions have been introduced within this context.

Within this field, an extensive overview is presented in [14], where a constitutive law was introduced to describe the rate-independent deformation of granular materials in soil mechanics. The laws are based on either plasticity or shearing theory and is valid for quasi-static regimes. Additionally, model for the collisional rapid flow of granular materials was presented in [15], based on the kinetic theory of dense gases. These two approaches have been instrumental in studying the transitional regime, which encompasses both collisional and frictional responses [16]. However, it is essential to note that these models have primarily focused on spherical grains to simplify geometrical consideration.

The majority of granular flows, in practice, involve non-spherical grains and most grains possess some degree of asphericity. Extensive numerical and experimental research has been conducted to investigate the profound impact of grain shape on

granular flow. Current models in this field tend to focus on grain sizes, largely overlooking the shape of the grains and their impact on alignment and rheology during flow. Hence, the development of a concise model to explore how grain shape influences their orientation and alignment during flow becomes crucial. From the results presented in [17, 18], it reveals that grain shape significantly influences grain orientation and mechanical response. In general, non-spherical grains exhibit more complex behavior compared to their spherical counterparts. Moreover, their inter-grain and microscopic interactions can occur on their surface area, in contrast to spherical grains, which interact at a point. Due to the collisional interactions among non-spherical grains, they tend align with the direction of the flow [19]. Furthermore, axisymmetric grains have a tendency to align along their larger dimension in the direction of the flow, as this alignment reflects the orientation of the ellipses [20].

Nadler et al. [21] proposed a kinematic model that establishes a connection between the flow and grains orientation. This model has the capacity to predict the average grains orientation based on the velocity field and the shape of the grains. Furthermore, it successfully captured the evolution of grain alignment and the tendency of non-spherical grains to align with each other during transitions.

To facilitate modelling the non-spherical grains, the work proposed in [21] expands the grains orientation model beyond spherical grains to accommodate ellipsoidal shapes. This new grain orientation model characterizes the length of each grain, as illustrated in Figure 1.3.

The parameters l and w represent the geometrical length and width of axisymmetric grains. An aspect ratio also was defined as

$$r_g = \frac{l - w}{l + w}, \tag{1.1}$$

which can vary within the range of -1 to 1, where $r_g = 0$ describes spherical grains.

This aspect ratio is positive and increasing with the elongation of prolate grains, where $l > w$, and it is negative and decreasing with the flatness of oblate grains, where $w > l$.

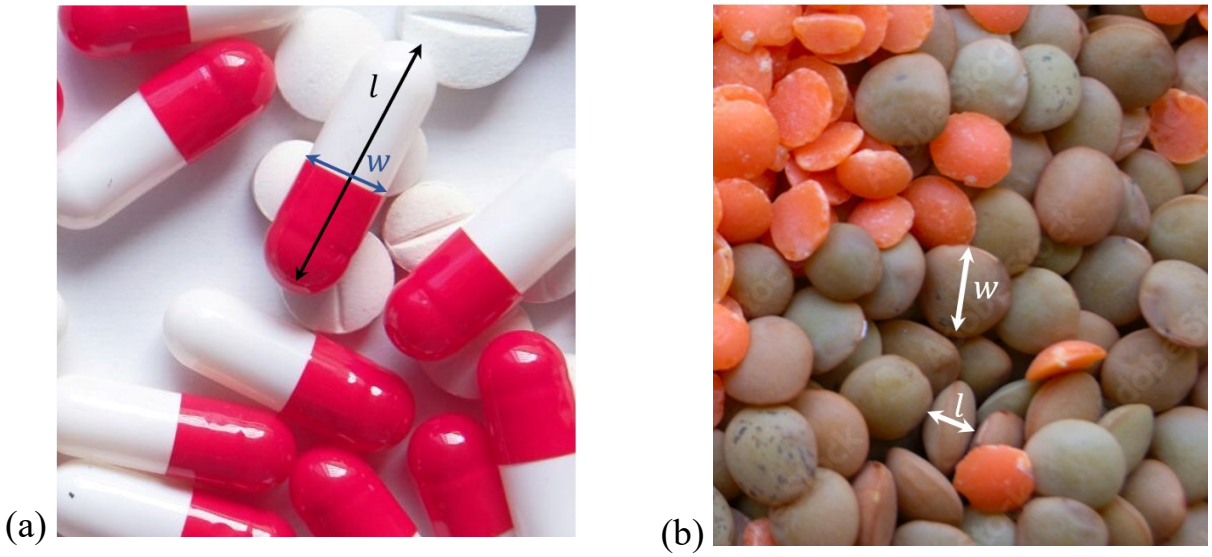

Figure 1.3. Examples of ellipsoidal grains, with (a) representing prolate grains like capsules, and (b) oblate grains like lentils.

The kinematic model presented in [21] was then verified with Discrete Element Method (DEM) simulations, a technique used for modeling the motion and interactions of grains, involve the explicit consideration of each grain and the interactions between them in terms of contacts and collisions. It was shown that the model well agreed with the simulations. However, it is worth noting that the model was primarily examined in homogeneous steady-state simple shear flow, but transient shear flows were also examined. A rheology model also was proposed that accounts for the microstructure orientation [22]. The model's performance in inhomogeneous flows, where grains orientations and velocities vary within the flow, is studied in [24] and a model is extended. The extension of the model introduced a capability to consider inhomogeneous orientational fields, characterized by spatial non-convective orientational flux. This flux accounts for the interactions of grains with their surroundings and boundaries. The model was then applied to investigate

the influence of orientational diffusion and boundary conditions on the flow of dense granular material down an incline, with the findings demonstrating the significant role played by the boundary conditions in determining grains orientations in such flows.

Experimental research has also demonstrated that changing the grain aspect ratio results in a significant impact on the flow rate of the grains. This can lead to jamming, which is a transition from an easily flowing state to a rigid jammed state and occurs more readily compared to spherical grains [24]. Furthermore, it is noted in [25] that non-spherical grains can achieve higher packing densities than their spherical counterparts. This is mainly attributed to disordered packing, wherein the volume fraction of grains decreases as the aspect ratio increases.

Furthermore, as an important application, hoppers have a long history of use for storing and handling bulk materials in various sectors. Failures in these systems often occur due to inadequate design analysis of the dynamic behavior of bulk material during hoppers discharge [26]. Common issues associated with hopper granular flow such as funnel flow, where grains flow through the core of the hopper while remaining at rest on the sides, leading to a wide residence time distribution and deterioration in product quality [27]. To enhance our comprehension of granular flow in these systems, different approaches have been explored. These include numerical modeling techniques such as the Finite Element Method and Discrete Element Method, as well as experimental tests conducted at both full and reduced scales. In an experiment in [28], both spherical and non-spherical granular flows were explored within rectangular hoppers using dynamic X-ray radiography. By using glass beads as spherical grains and comparing them with Jasmine rice and red lentils as non-spherical grains, the study investigates the influence of material choice and opening size on the flow regime. This exploration involves measuring the orientation and velocity of grains, revealing notable effects on the overall flow

behavior.

In the exploration of jamming probability in cylindrical hoppers, [29] focuses on the critical radius for the hopper opening. While this critical radius remained constant for spherical grains, it is dependent on the ratio of opening size to grain size for non-spherical grains. Shape, rather than material properties, emerged as a significant factor influencing arch formation and, consequently, the probability of jamming. All the studies show that the flow mechanisms in a hopper are quite complex and vary in time and space. The characteristics of the flow are likely to be influenced by the material and geometric properties of the hopper and boundary texture [30].

While numerous models have been assessed, the flow of non-spherical grains, specifically considering the effect of boundaries on flow in complex domain geometries, has not been thoroughly investigated. Given the limitations in experimental studies, it is imperative to evaluate the performance of the existing models in real-world applications with various domain geometries and boundary conditions, using effective and versatile Finite Element Method for simulating the flow of non-spherical grains in a hopper. This assessment will allow us to gauge the model's accuracy in scenarios featuring non-spherical granular flows with varying spatially grains orientations in practical applications.

1.3. Objectives

This study aims to use models of non-spherical grains, presented in [22, 23], to simulate the flow of non-spherical granular materials in a hopper. To achieve this, the governing equations have been implemented and inserted into a Finite Element Analysis suite through using the predefined modules and creating new modules in the suite.

The main objectives of this study include:

- Implementing the model ensuring compatibility with the modeling suite,

enabling simulation execution under various flow conditions, to evaluate the velocity and orientation fields.

- Simulation a similar problem as an experiment to assess the accuracy of the implementation.
- Investigating the influence of the model parameters on grains orientation and flow within a hopper.
- Studying the effect of boundary conditions on grains orientation and the flow.
- Providing an assessment on non-spherical granular flows within a hopper employing a finite element modelling package as a basis for future research in complex geometries and flow conditions, with applications of industrial storage and material handling.

A comparison with an experimental study will be presented to ensure the validity of the simulation and further studies on different geometry and boundary conditions are conducted to examine the capability of the model and to show the viability of the simulation to more complex problems in practical applications.

1.4. Thesis Outline

This thesis is organized into five chapters, each of which contributes to the overall understanding of the subject. A brief overview of the following chapters is as follows:

Chapter 2: Mathematical Model

In this chapter, the mathematical model that underpins the study is presented. The equations derived in [21, 22] are detailed, elaborating on all related model parameters and the underlying theoretical principles while adapting the equations to a two-dimensional study.

Chapter 3: Finite Element Analysis Implementation

This chapter includes the FEA suite implementation and configuration, focusing on the suite requirements for simulations. This section covers the implementation of the model, the definition of essential parameters, the description of various boundary conditions, and the required configuration for the simulation.

Chapter 4: Simulation, Results, and Discussion

This chapter is dedicated to analyzing the results obtained from implementing the FEA package under various conditions. This chapter explores the role of model parameters on the velocity profiles, and grains orientation. To validate the simulation, the aim is to compare the findings with an existing experiment of simple hopper flows and extend the study to different geometries and conditions.

Chapter 5: Conclusions and Future Works

The final chapter offers a concise summary of the key findings and conclusions derived from this study. The conclusion contains proposing potential avenues for future research, envisioning ways to further develop this concept and extend its practical applications.

Chapter 2

2. Mathematical Model

As mentioned previously, most of the existing continuum models for granular flows are primarily valid for spherical grains. However, non-spherical grains exhibit more intricate mechanical behaviors due to their capability to orient with respect to each other. Additionally, the initial orientations and boundary conditions of these grains and their evolution over time significantly influence their mechanical responses. In the next section the previously developed model for non-spherical grains will be introduced in order to implement the equations in the present study.

2.1. The Orientation Balance Law

In [21], a method for representing the shape of ellipsoidal grains was introduced as a means to define grains orientations. Subsequently, the model was established based on these grain shapes. This approach led to the determination of two model parameters, both of which are dependent on the specific grain shape. The continuum model was initially compared with Discrete Element Method simulations and the results indicated a favorable agreement between the model and DEM simulations in homogeneous steady-state conditions. In the study, the model does not consider inhomogeneous flow and an extended model is proposed in [23].

A method was developed to individually define each non-spherical grain by considering its orientation, taking into account the grain's length and diameter, and its orientation which can be represent by a unit vector. This unit vector aligns with the grain's symmetry axis and is crucial for determining the orientation of each grain.

To represent the statistical orientation of grains at a specific point in space and time, a symmetric probability density function denoted as $f(\mathbf{k})$ is introduced, where $\mathbf{k}$ is the unit vector and $f(+\mathbf{k}) = f(-\mathbf{k}) \geq 0$. Given that the focus of this study is on

two-dimensional geometries, the model is introduced within a two-dimensional setting. The integral of the probability density function over a unit ring is

$$\oint_s f(\mathbf{k})\, da = 1. \tag{2.1}$$

In essence, the unit ring encapsulates all potential orientations of the unit vector $\mathbf{k}$ and the sum of possibilities for orientation across the ring is unity. To effectively describe the grains orientation distribution, the second order tensorial moment of $f(\mathbf{k})$ is utilized, as denoted by the equation

$$\mathbf{A} = \oint_s f(\mathbf{k})\mathbf{k} \otimes \mathbf{k}\, da, \tag{2.2}$$

where $\otimes$ is a tensor product operator and this expression quantifies the grains orientation distribution over the unit ring. It is clear from the definition that the orientation tensor $\mathbf{A}$, is a positive semi-definite and symmetric tensor. Using the symmetry property of $\mathbf{A}$, the spectral representation is

$$\mathbf{A} = \sum_{i=1}^{2} a_{\mathrm{i}}(\mathbf{a}_{\mathrm{i}} \otimes \mathbf{a}_{\mathrm{i}}), \tag{2.3}$$

where a_{i} are the eigenvalues of $\mathbf{A}$, with $0 \le a_1 \le a_2 \le 1$ and $a_1 + a_2 = 1$, and $\mathbf{a}_{\mathrm{i}}$ are the associated eigenvectors. Because $\mathbf{A}$ is a symmetric tensor, its eigenvalues are real, and the corresponding eigenvectors are mutually orthogonal.

In Figure 2.1, an ellipsoid depicts the orientation tensor. This representation is used to display both the eigenvalues and their respective eigenvectors.

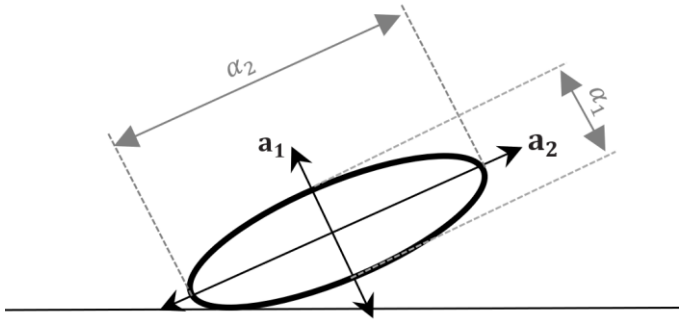

Figure 2.1. Eigenvalues a_1, a_2 and associated eigenvectors $\mathbf{a_1}$, $\mathbf{a_2}$.

The model that predicts the evolution of the orientational tensor is based on the velocity field, in which the velocity gradient $\mathbf{L}$ is defined as

$$\mathbf{L} = \text{grad}\mathbf{v}, \tag{2.4}$$

where $\mathbf{v}$ represents the velocity field. The velocity gradient can be decomposed to its symmetrical part, $\mathbf{D}$, and its antisymmetric part, $\mathbf{W}$, such that $\mathbf{L} = \mathbf{D} + \mathbf{W}$, and these two parts are defined as

$$\mathbf{D} = \frac{1}{2}(\mathbf{L} + \mathbf{L}^T) = \mathbf{D}^T, \tag{2.5}$$

$$\mathbf{W} = \frac{1}{2}(\mathbf{L} - \mathbf{L}^T) = -\mathbf{W}^T, \tag{2.6}$$

where $\mathbf{D}$ signifies the rate of deformation and $\mathbf{W}$ represents the vorticity. The rate of change of the orientation tensor $\mathbf{A}$ is described with by material parameters, in a two-dimensional context as

$$\dot{\mathbf{A}} = \mathbf{WA} - \mathbf{AW} + \lambda[\mathbf{AD} + \mathbf{DA} - 2(\mathbf{A}\cdot\mathbf{D})\mathbf{A}] - \psi \mathrm{D}'\left(\mathbf{A} - \frac{\mathbf{I}}{2}\right) + \text{div}\,[\alpha \mathrm{D}'\text{grad}\mathbf{A}], \tag{2.7}$$

where $\dot{\mathbf{A}}$ is the material time derivative of the orientation tensor, $\mathbf{I}$ represents the identity tensor, and D' is the magnitude of the deviatoric part of the rate of deformation and defined as

$$\mathrm{D}' = \sqrt{\mathbf{D}' \cdot \mathbf{D}'}, \tag{2.8}$$

where $\mathbf{D}'$ is the deviatoric part of the rate of deformation expressed as

$$\mathbf{D}' = \mathbf{D} - \frac{1}{2}\,\text{trace}(\mathbf{D})\mathbf{I}. \tag{2.9}$$

The two model parameters, λ and ψ, characterize the tendency of alignment of the grains and relaxation toward isotropic distribution, respectively. It was shown in [21] that these two parameters can be taken to be a function of the aspect ratio r_g.

The model parameter λ takes the range of [-1, 1]. For spherical grains $\lambda = 0$. As grains become more aspherical, $|\lambda|$ increases. When $|\lambda| \to 1$, one grain dimension

becomes significantly smaller than the other. For prolate grains, λ is positive while for oblate grains, λ is negative.

The material parameter ψ represents the effect of misalignment caused by grain collisions which is taken to be proportional to the magnitude of shear rate. Since the tendency of the grains to orient due to collision is toward random distribution, ψ is a non-negative parameter. Furthermore, ψ is expected to be smaller for higher degree of asphericity as such grains tend not to easily misalign. In other words, ellipsoidal grains can collide and interlock, reducing the misalignment effect caused by collisions on grains orientation. The numerical values for λ and ψ were proposed in [21] and will be used later.

Furthermore, to account for interactions through collisions and contacts with the surroundings, the inhomogeneous orientation field has been related to orientational diffusion. To include such orientational diffusion, the evolution equation was generalized by adding a diffusion flux. In this context, the term $\alpha \mathrm{D}' \mathrm{grad}\mathbf{A}$ presents in equation (2.7), where α is the orientational diffusion coefficient that possesses dimensions of length squared. The diffusion flux is taken to be proportional to the spatial gradient of the orientation, as diffusion occurs due to collisions.

2.2. The Influence of Orientation on the Rheology

The relationship between rheological stress and the flow is explained by a constitutive law that dictates the stress $\boldsymbol{\sigma}$ arising within the flow. This relationship in a macroscopic scale is a manifestation of the interactions taking place between grains at the microscopic level, which include factors such as grain shape, roughness, orientation, and flow. In this study, an inertia rheology model for incompressible flow is employed, as initially proposed in [22].

$$\boldsymbol{\sigma} = \boldsymbol{\sigma}\left(I, \mathrm{p}, \mathbf{D}, \mathbf{A}; r_g\right) = -\mathrm{p}\mathbf{I} + \mathrm{p}\mu(I)\varphi\left[\overline{\mathbf{D}} + \eta\left[\mathbf{A}\overline{\mathbf{D}} + \overline{\mathbf{D}}\mathbf{A} - \frac{2}{3}(\mathbf{D}\cdot\mathbf{A})\mathbf{I}\right]\right], \qquad (2.10)$$

where $\bar{\mathbf{D}} = \mathbf{D}/\sqrt{\mathbf{D}\cdot\mathbf{D}}$ represents the direction of the rate of deformation while the dominator is the magnitude of the rate of deformation. In this equation $\mu(I)$ denotes the friction. The phenomenological inertia rheology relation is given by

$$\mu(I) = \mu_s + \mu_1 I^{\beta}, \tag{2.11}$$

where μ_s, μ_1 and β are phenomenological parameters which obtained from experiments and depend on grains shape and interfacial friction between them. This equation is an extension of the isotropic inertia rheology [31], which relies on the dimensionless inertia number,

$$I = \mathrm{D}d/\sqrt{\mathrm{p}/\rho_s}, \tag{2.12}$$

where d is grain diameter, p is the pressure, and ρ_s is the solid density. For non-spherical grains, d will be the diameter of a sphere with the same volume as a grain.

Furthermore, two other model parameters, $\varphi(r_g)$ and $\eta(r_g)$, were introduced in the stress equation and were assumed to be functions solely of the aspect ratio, r_g. The parameter $\varphi(r_g)$ is related to the effect of interlocking between ellipsoidal grains at isotropic orientation and is a correction for the deviation from spherical grains for $\mu(I)$. The parameter $\eta(r_g)$ relates to the effect of grains alignment and is expected to be negative yielding reduction in the slip resistance on alignment plan and to decrease monotonically with r_g. It governs the rheological response, predicting that the higher alignment of the axisymmetric grains with the flow leads to lower shear flow resistance along the planes of alignment. The parameter $\eta(r_g)$ is proposed in [22] and will be used later.

The equations for the conservation of mass and the balance of linear momentum are utilized to calculate the density ρ and velocity $\mathbf{v}$ fields,

$$\dot{\rho} + \rho \,\mathrm{div}\,\mathbf{v} = 0, \qquad \rho\dot{\mathbf{v}} = \rho\mathbf{b} + \mathrm{div}\,\boldsymbol{\sigma}, \tag{2.13}$$

where $\mathbf{b}$ is the body force and $\boldsymbol{\sigma}$ is the Cauchy stress and for non-spherical grains introduced as equation (2.10). This inertia rheology is applicable to incompressible

flow. To close the set of governing equations, conservation of mass and the balance of linear momentum supplemented by a constitutive law, where the constitutive law is an explicit function of the orientational tensor and couples the response of the system. The initial and boundary conditions for both velocity and orientation fields are essential for solving the conservation of mass and the balance of linear momentum and the orientation law, topics that will be elaborated upon in the subsequent section.

Chapter 3

3. Finite Element Analysis Implementation

This chapter explains the steps taken to integrate the equations of orientation balance law and anisotropic rheology model within a FEA suite and discusses the associated requirements for boundary conditions to conduct the simulation.

3.1. Model Implementation

To analyze the behavior of the flow influenced by orientation, it is necessary to solve the set of coupled governing equations (2.7) and (2.10) for the conservation of mass and the balance of linear momentum, along with the equation for the evolution of orientation under different conditions. For this purpose, equations (2.7) and (2.10) need to be integrated into a FEA suite to be coupled and solved together.

The chosen FEA suite for this simulation is COMSOL Multiphysics®[32], selected for its versatility in modifying predefined equations and incorporating new ones as well as creating modules for solving new physics [33]. While COMSOL Multiphysics features versatile modules, integrating the specific equations posed challenges. Addressing and overcoming these limitations constituted a significant portion of this thesis.

COMSOL Multiphysics offers predefined modules for implementing equations, however the introduced equations, encompassing the balance of momentum and the orientation balance law, do not align with standard equation formats within the suite. Modifying these predefined equations in COMSOL Multiphysics is constrained. To address this, we adapted the balance of linear momentum equation to incorporate the inertia rheology model. Since predefined modules also have their limitation in terms of the format of equations, making the adjustment between the existing model and the equation forms in COMSOL Multiphysics is challenging.

In solving the balance of linear momentum, the single-phase flow module has been employed with the following standard formulation,

$$\rho\frac{\partial \mathbf{v}}{\partial t}+\rho\mathbf{v}\cdot\mathrm{grad}\mathbf{v}=\mathrm{div}[-\mathrm{p}\mathbf{I}+2\mu\mathbf{D}]+\mathbf{F}+\rho\mathbf{g}\,, \tag{3.1}$$

where $\mathbf{v}$ is velocity field, ρ density, p pressure, μ is the media viscosity, $\mathbf{F}$ volume force, and $\rho\mathbf{g}$ is body force. To incorporate equation (2.10) into this equation, the term $[-\mathrm{p}\mathbf{I}+2\mu\mathbf{D}]$ should ideally be replaced by equation (2.10). However, COMSOL Multiphysics does not allow for the modification of this term. The only adjustable element in this equation is the volume force, $\mathbf{F}$. So, we need to eliminate the deviatoric stress, $2\mu\mathbf{D}$**,** in equation (3.1), to unify the momentum equation with the influence of the inertia rheology model. Subsequently, we take the gradient of the deviatoric stress in equation (2.10) and substitute the $\mathbf{F}$ term as follows,

$$\mathbf{F}=\mathrm{div}\left(\mathrm{p}\mu(I)\varphi\left[\overline{\mathbf{D}}+\eta\left[\mathbf{A}\overline{\mathbf{D}}\ +\overline{\mathbf{D}}\mathbf{A}-\frac{2}{3}(\mathbf{D}\cdot\mathbf{A})\mathbf{I}\right]\right]\right), \tag{3.2}$$

and the final form of equation of balance of linear momentum in the simulation is

$$\rho\frac{\partial \mathbf{v}}{\partial t}+\rho\mathbf{v}\cdot\mathrm{grad}\mathbf{v}=\mathrm{div}\left[-\mathrm{p}\mathbf{I}+\mathrm{p}\mu(I)\varphi\left[\overline{\mathbf{D}}+\eta\left[\mathbf{A}\overline{\mathbf{D}}+\overline{\mathbf{D}}\mathbf{A}-\frac{2}{3}(\mathbf{D}\cdot\mathbf{A})\mathbf{I}\right]\right]\right]+\rho\mathbf{g}\,. \tag{3.3}$$

This configuration allows us to solve the momentum equation valid for non-spherical granular materials.

An additional module needs to be defined for the equation of evolution of orientation, and equation (2.7) should be integrated into this module. One of the options for this purpose is using a 'General Form PDE Mathematical' module with its predefined formulation in COMSOL Multiphysics, as outlined below:

$$e^{a}\frac{\partial^{2}\mathbf{A}}{\partial t^{2}}+d_{a}\frac{\partial \mathbf{A}}{\partial t}+\mathrm{div}\boldsymbol{\Gamma}=\boldsymbol{f}. \tag{3.4}$$

In this equation, e^{a} and d_{a} are coefficients, while $\boldsymbol{\Gamma}$ and $\boldsymbol{f}$ are expressions, all of which can be defined. This flexibility allows for the adjustment of different

equations into the predefined format specified by this equation. Comparison with $\dot{\mathbf{A}}$, by setting $e^a = 0$, $d_a = 1$, and $\boldsymbol{\Gamma} = 0$, the left-hand side becomes $\partial \boldsymbol{A}/\partial \mathrm{t}$ which is the temporal part of the material time derivative of the orientation tensor. In this equation, $\boldsymbol{f}$, known as source term, is the only term capable of entering desirable equations into the predefined format. Given that the material time derivative of $\mathbf{A}$ is

$$\dot{\mathbf{A}} = \frac{\partial \mathbf{A}}{\partial t} + (\mathrm{grad}\ \mathbf{A})\mathbf{v}, \tag{3.5}$$

by taking $-(\mathrm{grad}\ \mathbf{A})\mathbf{v}$ to the right-hand side of equation (2.7) and incorporating it into the term $\boldsymbol{f}$ in equation (3.4), it will be

$$\boldsymbol{f} = \mathbf{WA} - \mathbf{AW} + \lambda[\mathbf{AD} + \mathbf{DA} - 2(\mathbf{A}\cdot\mathbf{D})\mathbf{A}] - \psi \mathrm{D}'\left(\mathbf{A} - \frac{\mathbf{I}}{2}\right) + \mathrm{div}\,[\alpha \mathrm{D}' \mathrm{grad}\mathbf{A}] - (\mathrm{grad}\ \mathbf{A})\mathbf{v}. \tag{3.6}$$

With this configuration, the equation of orientation evolution is prepared to be coupled with the modified single-phase flow module. This adaptation enables the inclusion of the evolution law as a separate module within the suite.

The default settings in COMSOL Multiphysics for the set physics may not be suitable for conducting the solution. Due to the mutual dependency between the balance of linear momentum equation and orientation, the selection of the 'fully coupled' method is imperative for the simulation. This method forms a single large system of equations that solve for all unknowns and includes all couplings between them in a single iteration. This is in contrast to the 'segregated' method, selected by COMSOL Multiphysics for two-dimensional simulations, which subdivides the problem into two or more Segregated Steps. The 'fully coupled' approach often converges more robustly and in fewer iterations compared to the Segregated approach. However, each iteration will require more memory and time to solve.

3.2. Boundary Conditions

The evolution law in equation (2.7) represents an initial boundary-valued problem,

involving a first-order differential equation in time and a second-order differential equation in space. To solve this equation, proper initial and boundary conditions for $\mathbf{v}$ and $\mathbf{A}$ are necessary. The initial value of $\mathbf{A}$ within the domain must be specified as the initial conditions, which is considered to be isotropic, i.e., a same probability of orientation in all directions. Furthermore, specifying boundary conditions is crucial, as they can significantly affect the orientational field and the associated flow in steady state. These boundary conditions can be of the Dirichlet type (imposing the value of $\mathbf{A}$), Neumann type (imposing the value of the directional derivative of $\mathbf{A}$), or a mixed type.

The interaction of grains with the boundary is influenced by the surface properties, grains orientation, and the flow, which can lead to grain alignment with the boundary surface by providing orientational flux. In this study, for simplicity, no jump on boundaries is considered; that is, the orientation of the grains in contact with the boundary is completely aligned with the boundary.

To obtain the boundaries orientation taken as the orientation of grains forming the boundary, the following approach have been considered. A wall with an angle γ with respect to the vertical downward flow is depicted as a dashed line in Figure 3.1. The orientation of the unit vector tangent to the wall, as illustrated in the figure, can be determined as follows:

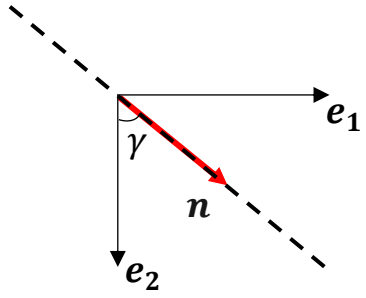

Figure 3.1. A unit vector, $\boldsymbol{n}$, normal to a wall, with an angle of γ with respect to the flow direction

$$\boldsymbol{n} = (\sin\gamma \boldsymbol{e_1} + \cos\gamma \boldsymbol{e_2}), \tag{3.7}$$

where, $\boldsymbol{e_1}$ and $\boldsymbol{e_2}$ are unit vectors representing two orthogonal directions in space.

Applying a tensor product operator to this unit vector with itself allows us to determine the orientation of the wall. The orientation tensor for the wall can be expressed as follows:

$$\begin{aligned} &\mathbf{A}_w = \boldsymbol{n}\otimes\boldsymbol{n}, \\ &\mathbf{A}_w = \sin^2\gamma(\boldsymbol{e}_1\otimes\boldsymbol{e}_1) + \cos^2\gamma(\boldsymbol{e}_2\otimes\boldsymbol{e}_2) + \cos\gamma\sin\gamma(\boldsymbol{e}_1\otimes\boldsymbol{e}_2 + \boldsymbol{e}_2\otimes\boldsymbol{e}_1). \end{aligned} \tag{3.8}$$

By setting the orientation evolution law with a no-jump boundary condition, coupled with the conservation of mass and the balance of linear momentum, supplemented by the introduced constitutive law, along with a no-slip boundary condition for velocity, the set of governing equations is closed.

3.3. Orientation Distribution

To represent the orientational field, the orientational angle is introduced based on eigenvectors of the tensors. By taking into account the components of the eigenvector, the preferred orientation, represented as the angle of the largest eigenvalue with respect to the flow direction, can be defined as follows,

$$\theta = \tan^{-1}\frac{\mathrm{a}_2{}^y}{\mathrm{a}_2{}^x}, \tag{3.9}$$

where $\mathrm{a}_2{}^y$ and $\mathrm{a}_2{}^x$ are the components of the associated eigenvectors, in x and y directions respectively, to the larger aspect of the grains.

An additional useful alignment measure is the ordering factor [23,34], which represents the mutual alignment of grains. It is defined as

$$\zeta = |a_2 - a_1|, \tag{3.10}$$

where $0 \leq \zeta \leq 1$, such that, $\zeta = 0$ represents the isotropic distribution of the grains, with all eigenvalues $a_1 = a_2 = 0.5$. When $\zeta = 1$, it represents the maximum alignment of the grains, where all grains are aligned along one direction. In this case,

one of eigenvalues approaches zero ($a_1 \to 0$), and the other one approaches one ($a_2 \to 1$).

In the next chapter, the results of simulating the flow of non-spherical grains using the discussed model are presented. The findings are detailed for the velocity field, orientational angle, and ordering factor as previously introduced.

Chapter 4

4. Simulation, Results, and Discussion

After implementing the model into the suite with the governing equations and setting the initial and boundary conditions, simulations were conducted, and the results for velocity and orientation fields under different conditions were obtained. This chapter is dedicated to presenting and discussing the obtained results. The chapter is divided into two sections. First, to validate the implementation in COMSOL Multiphysics and to assess the model performance, a similar experimental study is chosen for simulation, and the results are then compared with experimental data. The subsequent section provides detailed information on this particular case. Second, the simulation's viability is investigated in more intricate geometries and under varied conditions.

4.1. Comparison with Experiments

In [28], an experiment was conducted to investigate the flow of both spherical and non-spherical granular flows within a rectangular hopper. The primary objectives were to measure the velocity field, and orientation of grains utilizing a method as X-ray radiography.

The hopper, with dimensions of $\mathrm{H} = 300$ mm in height and $\mathrm{L} = 130$ mm in length, featured two distinct opening sizes ranging from $\mathrm{W}_1 = 10$ mm to $\mathrm{W}_2 = 15$ mm. Spherical glass beads and non-spherical grains, specifically Jasmine rice and red lentils, were employed in the experiment. The discharge process was initiated by releasing a trapdoor mechanism after filling the hopper with grains. Following a brief transient period, the material discharged at a constant rate. Temporal averages of grain orientation and velocity field measurements were conducted during this phase of steady discharge.

To validate the integrated model in COMSOL Multiphysics and the implementation made, a simulation with a similar setting was conducted. For this purpose, a same specification was selected to simulate the case that was studied in [28]. A two-dimensional rectangular hopper was selected, depicted in Figure 4.1, with introduced height and length, and the investigation was carried out for two opening sizes: 10 mm and 15 mm, for two types of non-spherical grains - Jasmine rice, and red lentils. To account for the shape of grains, the model parameters λ, ψ, and η are calculated based on the definition provided in the proposed model [22] as follows

$$\begin{aligned} \lambda(r_g) &= \left(2/\pi\right)\tan^{-1}(5.5r_g), \\ \psi(r_g) &= 0.85\exp(-4{r_g}^2), \\ \eta(r_g) &= 0.746\tan^{-1}(4.226r_g). \end{aligned} \tag{4.1}$$

By definition, r_g is changing between -1 and 1. Additionally, the λ values increase between -1 and 1, while ψ is positive and varies between 0 and 1. So, it is expected that for $r_g > 0$, $\psi > 0$ and $0 < \lambda < 1$, and for $r_g < 0$, $\psi < 0$ and $-1 < \lambda < 0$ as they are considered to be the functions of r_g. Furthermore, there are constraints of $\eta > -1$ and $\varphi > 0$ to ensure compliance with the dissipation inequality as explained in [22].

Based on the aspect ratio of the grains in the experiment, the obtained model parameters are shown in Table 4.1.

Regarding the model parameter φ, since $\mu(I)\varphi$ is associated with the isotropic inertia rheology of non-spherical grains, and it is assumed here that all the frictional properties of the grains are already captured by the constants μ_1, μ_s, β in equation (2.11), φ is set to be φ=1 [22].

According to the definitions provided in chapter 1, the negative aspect ratio for red lentils shows that the length of these grains is shorter than their diameter.

Table 4.1. Calculating the model parameters based on the aspect ratios

Material	Density (kg/m3)	Aspect ratio	Model Parameters		
			$\boldsymbol{\lambda}$	$\boldsymbol{\psi}$	$\boldsymbol{\eta}$
Glass beads	1462	1.1	0.9	0.006	1
Jasmine rice	822	0.634	0.822	0.170	0.907
Red lentils	721	-0.475	-0.767	0.344	-0.829

The material is set as an incompressible fluid, and as mentioned earlier, a single-phase flow model was employed for the solution. For the bulk density of the medium, a fraction of 0.64 is considered, employed relative to the density of the solid, and this value is adopted from a previous study on granular materials [35].

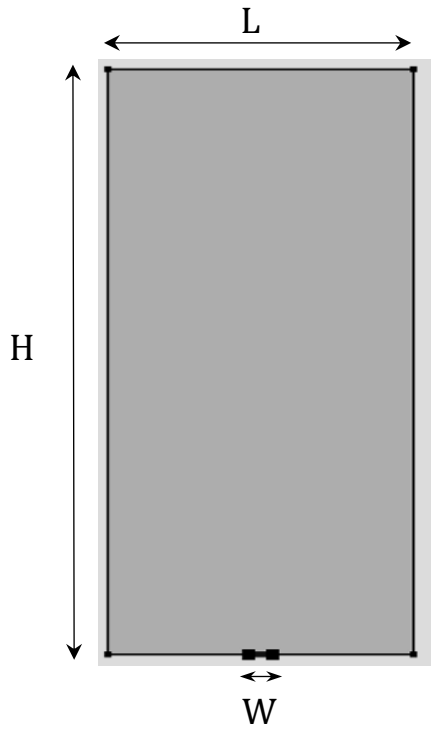

Figure 4.1. The hopper geometry used in the experimental study [28]

4.1.1. Boundary Conditions

The boundary conditions for the velocity field are no-slip condition enforced on the walls $\mathbf{v}_\mathrm{b} = 0$. The boundary orientation, $\mathbf{A}_\mathrm{b}$, represents the topology and orientation of the boundary surface. Here, we take no jump in boundary condition that is grains

in contact with the walls are in a full alignment with the orientation of the walls, i.e., $\mathbf{A}_{\mathrm{b}} = \mathbf{A}_{\mathrm{w}}$. To obtain the orientation of the walls, equation (3.8) has been utilized. Therefore, for vertical and horizontal walls, the following orientation boundary conditions are obtained for Jasmin rice, and red lentils.

$$\begin{aligned} &\text{Jasmin rice} \\ &\qquad \text{at Vertical walls: } \gamma = 0°,\ \mathbf{A}_w = 1(\boldsymbol{e_2}\otimes\boldsymbol{e_2}), \\ &\qquad \text{at Horizontal walls: } \gamma = 90°,\ \mathbf{A}_w = 1(\boldsymbol{e_1}\otimes\boldsymbol{e_1}), \\ &\text{Red lentiles} \\ &\qquad \text{at Vertical walls: } \gamma = 90°,\ \mathbf{A}_w = 1(\boldsymbol{e_1}\otimes\boldsymbol{e_1}), \\ &\qquad \text{at Horizontal walls: } \gamma = 0°,\ \mathbf{A}_w = 1(\boldsymbol{e_2}\otimes\boldsymbol{e_2}). \end{aligned} \tag{4.2}$$

It should be noted that the orientation of the unit vector for lentils is considered to have a 90-degree difference from that of rice. This distinction is based on the definitions of prolate and oblate grains provided in Chapter 1. Specifically, the unit vector for rice aligns with its length, while the unit vector for lentils is oriented normal to their flat surface.

4.1.2. Mesh Independence Study

A non-uniform mesh is considered and to capture a detailed variation of orientation near the walls, the mesh near the walls should be finer compared to the internal areas. Additionally, mesh independence is studied to make sure the solution does not change significantly by changing the number of meshes. For this purpose, as a starting point the meshing method is considered similar to the experimental setup in [28], hence the hopper is meshed with a suggested number of rectangular meshes as 'Normal' mesh for this geometry by COMSOL Multiphysics, depicted in Figure 4.2.

Then, mesh refinements are considered to calculate the average velocity at the outlet of the hopper. In line with best practices in CFD analysis, the criteria for the relative tolerance, defined as the tolerance between the results obtained by implementing two different set of meshes, is typically set to be less than 0.01% [36].

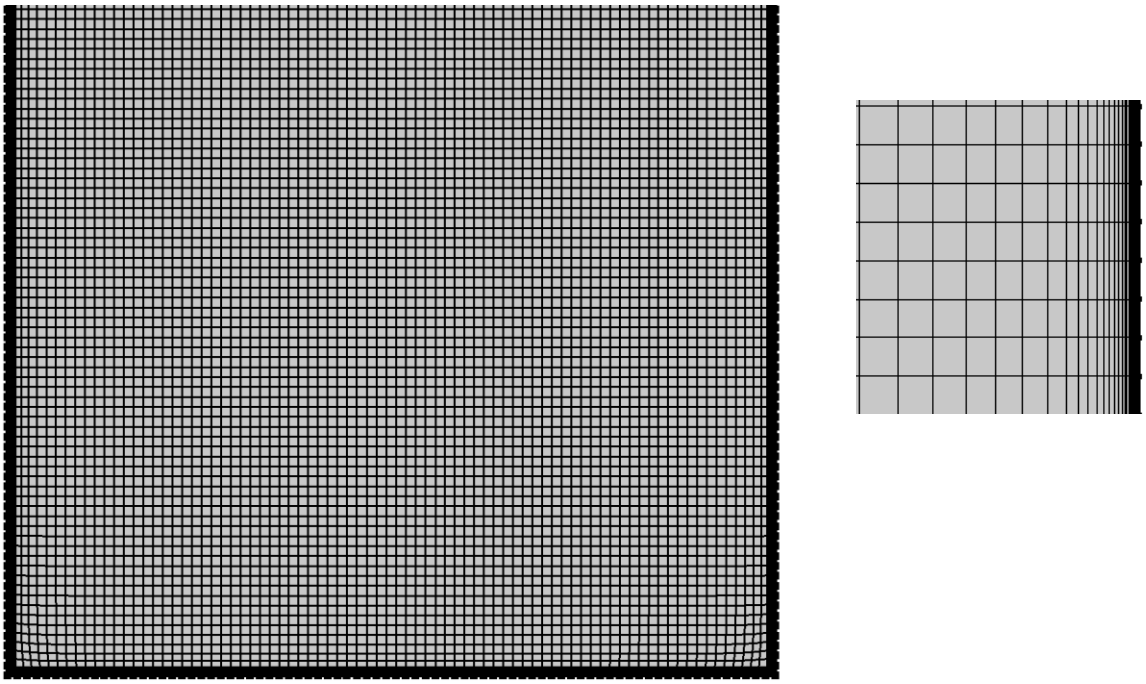

Figure 4.2. Rectangular meshes for the hopper geometry with finer meshes near the walls

As presented in Table 4.2, the difference between the converged values for average velocity using the initial two meshes exceeded this criterion. Consequently, mesh refinement was initiated according to the defined mesh refinements in the suite, and after three refinements, the tolerance was reduced to less than 0.01%. To mitigate the mesh's influence on the solution, the third arrangement was selected, as it yielded results that closely matched those obtained with the finest mesh while maintaining lower computational costs. With this number of nodes, it can be ensured that the size of the smallest mesh element is larger than the size of the grains, allowing each element to encompass multiple grains and effectively capture the collective behavior of the granular flow.

Table 4.2. Average velocity at the outlet of hopper in different meshes

Mesh	Number of Nodes	Converged value	Relative tolerance
1	9282	0.054833441	
2	12423	0.054614121	0.4000%
3	17660	0.054559562	0.0999%
4	28990	0.054554919	0.0085%

4.1.3. Analysis of Findings

Employing the introduced model, simulations were conducted for spherical glass beads, Jasmine rice, and red lentils, and results were obtained. A comparison between the simulation results and the experimental data is presented in Figures 4.3, 4.4, and 4.5.

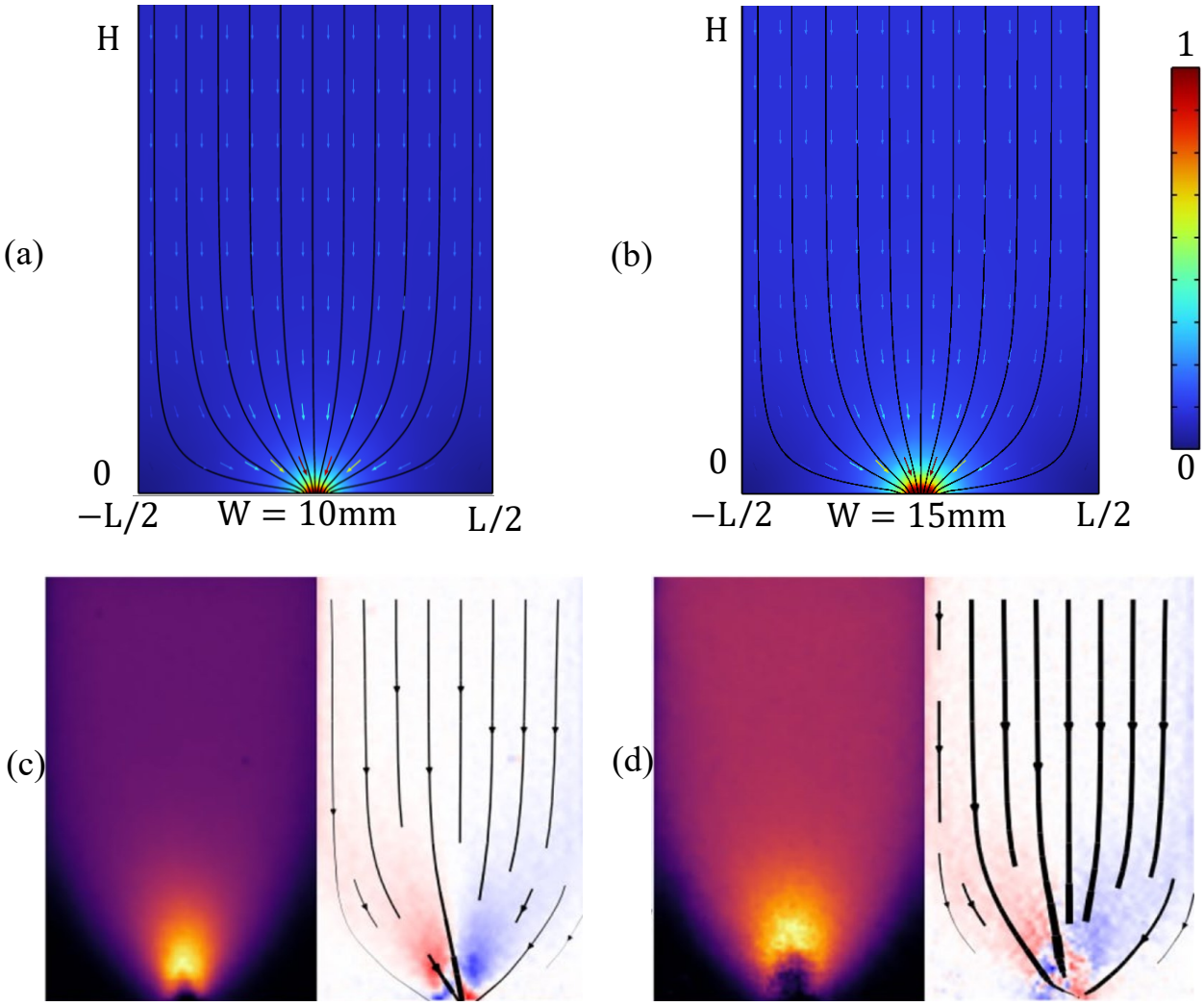

Figure 4.3. Comparison of the velocity field and streamlines for glass beads. (a), (b): simulation results, and (c), (d): experimental results. Normalization velocity for (a), (b) is 28.5, 37.4 (mm/s), respectively.

In Figures 4.3 (a) and (b), the velocity profiles, including streamlines and velocity field vectors for two different opening sizes, obtained from the simulation, are

compared with Figures 4.3 (c) and (d), which depict the measured velocity field and streamlines from the experimental study for glass beads. The same comparative order is maintained in Figures 4.4 and 4.5 for Jasmine rice and red lentils, respectively.

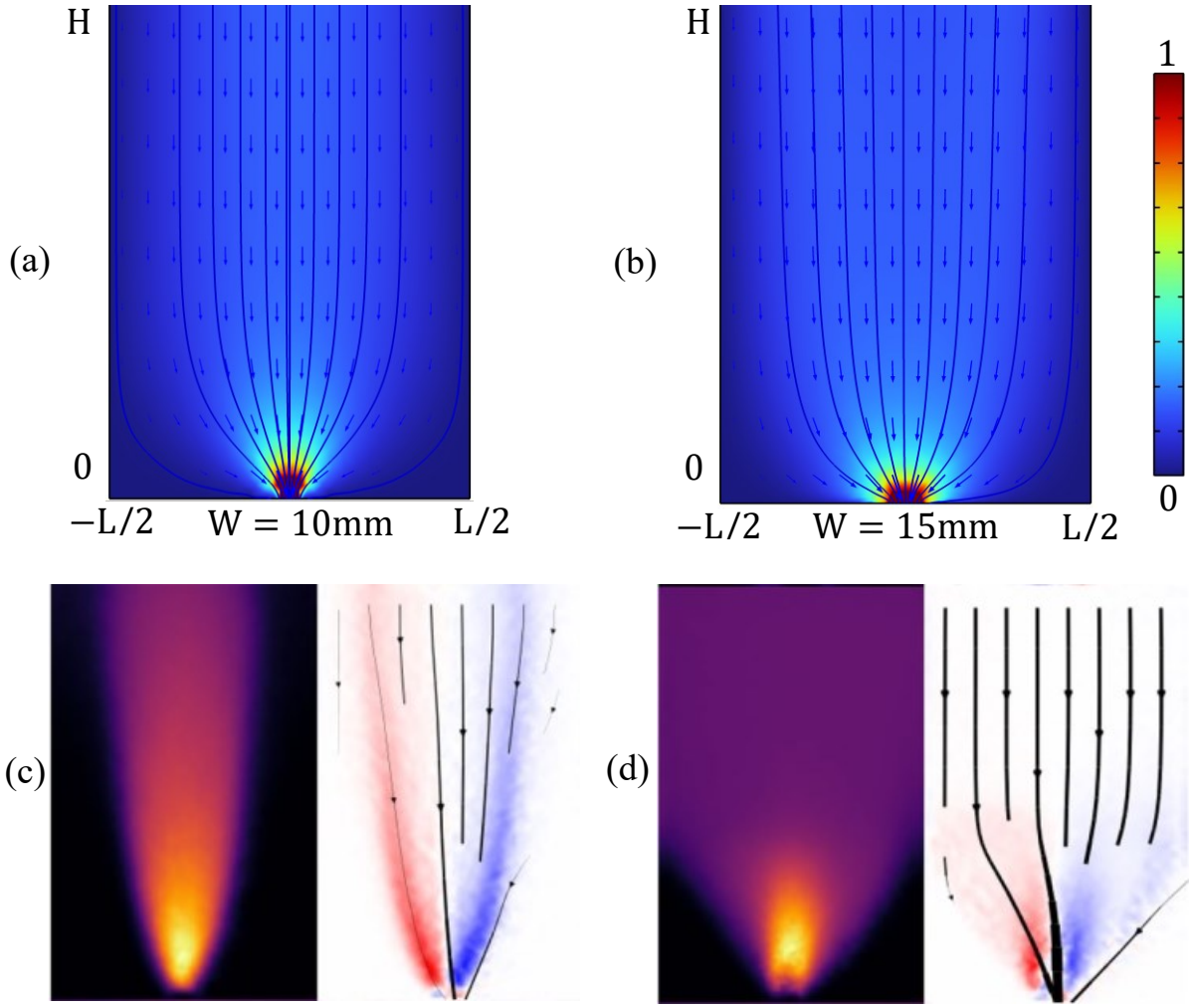

Figure 4.4. Comparison of the velocity and streamlines field for Jasmin rice. (a), (b): simulation results, and (c), (d): experimental results. Normalization velocity for (a), (b) is 18.4, 54.5 (mm/s), respectively.

Comparing figures 4.3, 4.4, and 4.5, the funnel flow regime is notably influenced by the grains shape and opening size, with stronger funneling observed for smaller openings. Funnel is a flow within the core of the hopper while the grains at both sides remain at rest. A comparison between figures 4.4a, 4.4b, and figures 4.5a, 4.5b

demonstrates that funnel flow is stronger with rice grains than with lentil grains, as the regions containing the grains with zero velocity at both sides of the hopper for rice are larger than those for lentils. This difference can be explained by the fact that rice grains have a more ellipsoidal shape compared to lentils, which means larger aspect ratio and larger values for model parameters causing rice grains to orient less with the flow. This leads to the conclusion that the orientation of lentils starts in the upper layers compared to rice.

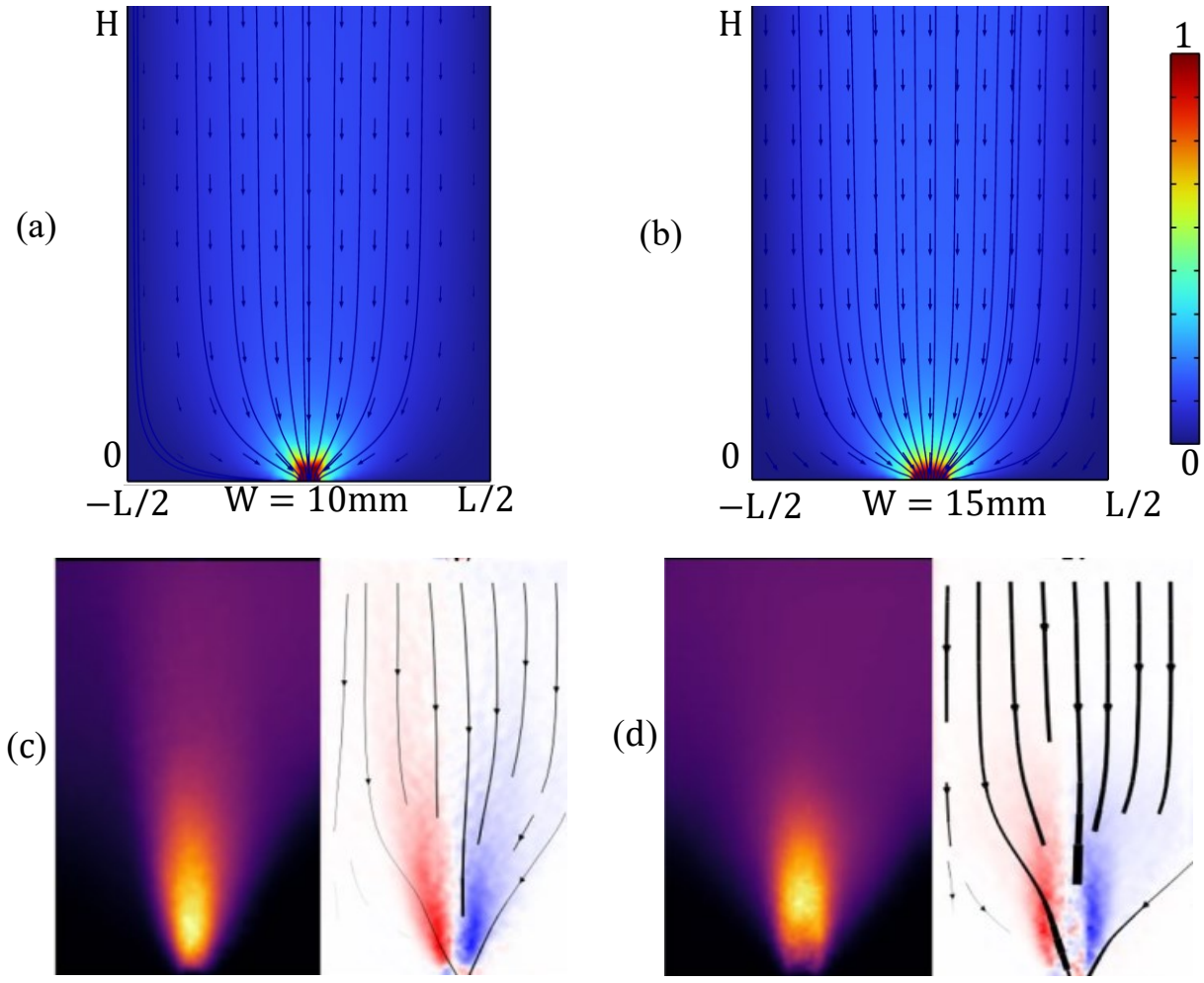

Figure 4.5. Comparison of the velocity field and streamlines for red lentils. (a), (b): simulation results, and (c), (d): experimental results. Normalization velocity for (a), (b) is 17.6 and 65.2 (mm/s), respectively.

Additionally, color maps and streamlines reveal that funnel flow takes place in the

hopper with the smaller opening, while bulk flow occurs in the hopper with the larger opening. Additionally, it is obvious that larger openings lead to higher velocity magnitude across the domain, accompanied by alterations in the streamline pattern.

Both the magnitude of velocity and the patterns of streamlines obtained from simulations align well with the experimental results, demonstrating the accurate and successful capture of the effects of model parameters.

Additionally, in [28], grain orientation was determined using X-ray radiography and Fourier transforms, employing steel tracer particles of the same size as the grains. Placed every two centimeters vertically in the center of the hopper, these steel tracer particles allowed for the measurement of grain orientation. It was observed that in the upper layers, grains typically lie horizontally due to the filling procedure. Moreover, in bulk flow, grains start to align with the flow stream when grains reach the openings. However, in funneling flow, grains begin to align farther upstream from the middle of the hopper.

Obtaining grain orientation from the solution of the model in the finite element suite reveals the following results for the same condition. Figure 4.6 illustrates the average orientation for Jasmin rice and red lentils for opening of W_1=10 mm, comparing the measured orientations using two different methods in the experiment and the results from the simulation. In the figure, the blue line represents the result from measuring the orientation of steel tracers during the flow, the red line indicates the orientation obtained from Fourier transform, and the green line displays the results for the orientational angle of grains located on a straight line from the inlet to the outlet of the hopper, obtained from the simulation.

As evident in the figures, at the top layer of the hopper, the grains are horizontal, transitioning to a more vertical orientation as the grains descend towards the opening. This observation is consistent with experimental findings for both Jasmin

rice and red lentils grains, confirming a strong agreement between the model results and experimental outcomes.

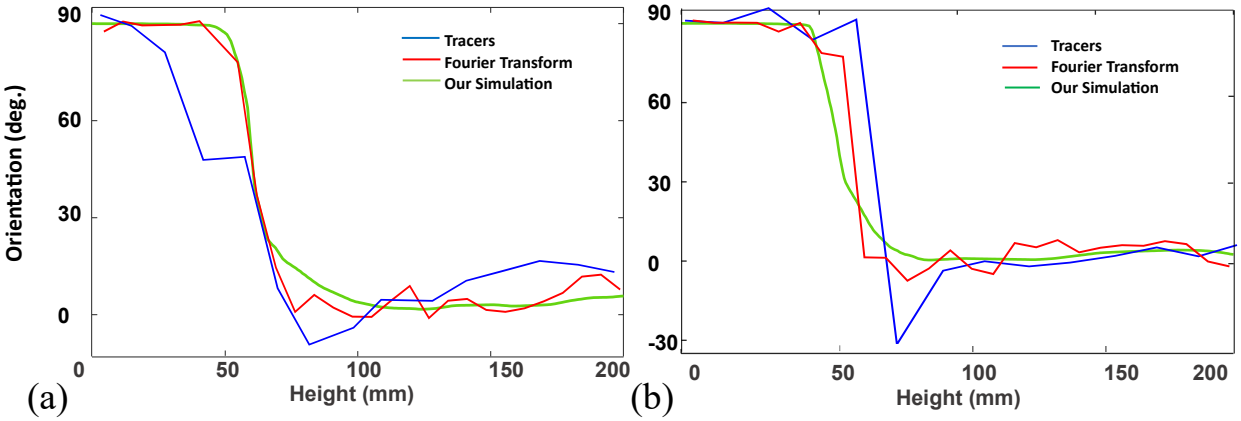

Figure 4.6. The orientation of grains for (a) Jasmin rice and (b) Red lentils. Note that considering the 90-degree difference in the orientation of the unit vector for lentils compared to that of rice, the adjustment has been made as per the experiment.

Comparing the rice and lentil orientation angle graphs show that the orientation of lentil starts at the upper height compared to rice. It leads to the conclusion that rice grains have a larger aspect ratio compared to the lentils, that cause grains to orient with the flow slower.

4.2. Extending the Study

Given that the results of simulations of the implemented model are in agreement with the experimental data, the demonstrated accuracy of the results validates the feasibility of extending the simulation to more complex geometries under various conditions. Moving forward, a study involving the investigation of different model parameters and various boundary conditions is being conducted to assess the model's capabilities and the practical application of the simulations. The results in this section in terms of the effect of boundary conditions, can be compared qualitatively with a previously conducted study, using the same model for a flow on an inclined surface [23].

The selected geometry for this investigation is a hopper with inclined walls, providing a more practical application in the field of granular materials storage. To examine the flow of non-spherical grains within the hopper, a simple 2-D hopper geometry is chosen, featuring two vertical walls, two inclined walls in the lower section, and two openings serving as the inlet and outlet, as illustrated in Figure 4.7, where the parametric dimensions of the hopper are outlined.

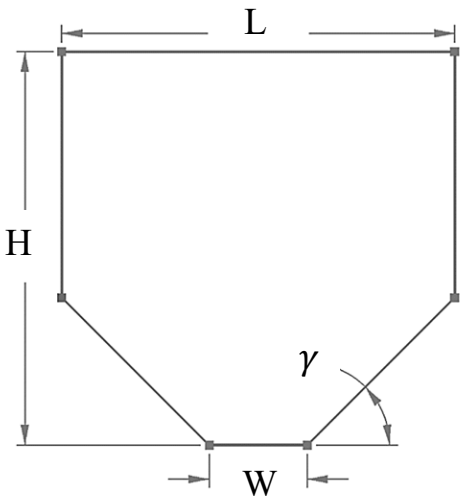

Figure 4.7. A simple 2-D hopper with parametric dimensions

4.3. Model Parameters and Characterization

For simplicity, we do not attempt to relate the model coefficients directly to the grain's properties and the flow, but rather consider them as constants, and their influence on the model predictions is investigated. A similar methodology in [33] is followed where, flows of cylindrical glass rods with a width w=1.9 mm and a length l=3.5w was studied which this leads to an aspect ratio of r_g= 0.55. By taking these values, for our simulation, we take the height of the flow to be significantly larger the grain size, $\mathrm{H}/w \approx 2 \times 10^2$, ensuring the applicability of a continuum model.

Based on the aspect ratio, the model parameter values, calculated using equation (4.1) as $\lambda = 0.8$, $\psi = 0.25$, and $\eta = -0.9$ show significant impacts on grain orientation and velocity field in the flow, as suggested in [21]. As these model

parameters are derived from experimental data, we refer to them as the 'Realistic Case' of model parameters. Additionally, to explore the influence of these model parameters, we compare the results with a 'Maximum Alignment Case' characterized by the least grains misalignment and an extreme tendency for alignment, achieved by setting the model parameters to $\lambda = 1$ and $\psi = 0$, where η considered the same in both cases.

These two sets of parameters illustrate their impact on the velocity field and orientation. In the following chapters, we will simply refer to these two sets of parameters as the Realistic Case and the Maximum Alignment Case to avoid repetition and for ease of reference.

The values of the parameters employed in the simulations are,

$$\beta = 1, \qquad \mu_s = 10^{-1}, \qquad \rho_s = 2500\ \mathrm{kgm}^{-3},$$
$$\varphi = 1, \qquad \mu_1 = 10^{-2}, \tag{4.3}$$

where the properties of the grains including shape, aspect ratio, and internal friction are represented by the model parameters which are taken from [22].

4.4. Boundary Conditions

The boundary conditions for the velocity field are no-slip condition enforced on the walls $\mathbf{v}_\mathrm{b} = 0$, where the grains are in direct contact with solid surfaces considering frictional interactions, and a constant average velocity inlet introduced into the hopper where $\mathrm{v}_\mathrm{in} = \mathrm{C}$, normal to the inlet plane, and grains exit into an environment at atmospheric pressure, $\mathrm{p}_\mathrm{out} = \mathrm{p}_\mathrm{atm}$.

Here again, as mentioned earlier, we take no jump in boundary condition and have the grains in contact with the walls aligned with the orientation of the walls, i.e., $\mathbf{A}_\mathrm{b} = \mathbf{A}_\mathrm{w}$. Two types of boundary orientation have been examined. First, for irregular boundary surface the boundary orientation takes an isotropic form, i.e., $\mathbf{A}_\mathrm{w} = \mathbf{I}/2$ at all walls, as depicted in Figure 4.8(a). In this type of boundary, named

'Rugged boundary', walls are not flat and grains on walls can orient randomly on walls.

Second, when the walls are flat and grains on the walls align with the orientation of the walls, it is referred as 'Flat boundary'. In this example, the inclined walls in the hopper section have a 45-degree angle as the chosen geometry is a simple example of a hopper, and this study does not intend to explore the impact of various hopper shapes and dimensions on the flow. Therefore, the orientation matrix for the left inclined wall can be imposed as follows:

$$at\ \gamma = 45°,\ \mathbf{A}_w = 0.5(\boldsymbol{e_1}\otimes\boldsymbol{e_1} + \boldsymbol{e_1}\otimes\boldsymbol{e_2} + \boldsymbol{e_2}\otimes\boldsymbol{e_1} + \boldsymbol{e_2}\otimes\boldsymbol{e_2})\ . \tag{4.4}$$

Using the same approach for other boundaries, the boundary conditions for both type of walls and when the orientation of the grains in contact with the boundary is completely aligned with the boundary are depicted in Figure 4.8(b). Therefore, the results in this section are divided into two categories based on the boundary types.

The results in the following section are normalized with respect to the height of hopper as the largest length in the domain.

$$\bar{y} = \frac{y}{\mathrm{H}}\ , \qquad \bar{x} = \frac{x}{\mathrm{H}}\ , \qquad \bar{\alpha} = \frac{\alpha}{\mathrm{H}^2}\ , \qquad \bar{\mathrm{v}} = \frac{\mathrm{v}}{\mathrm{H}}\ , \tag{4.5}$$

where v is the magnitude of velocity.

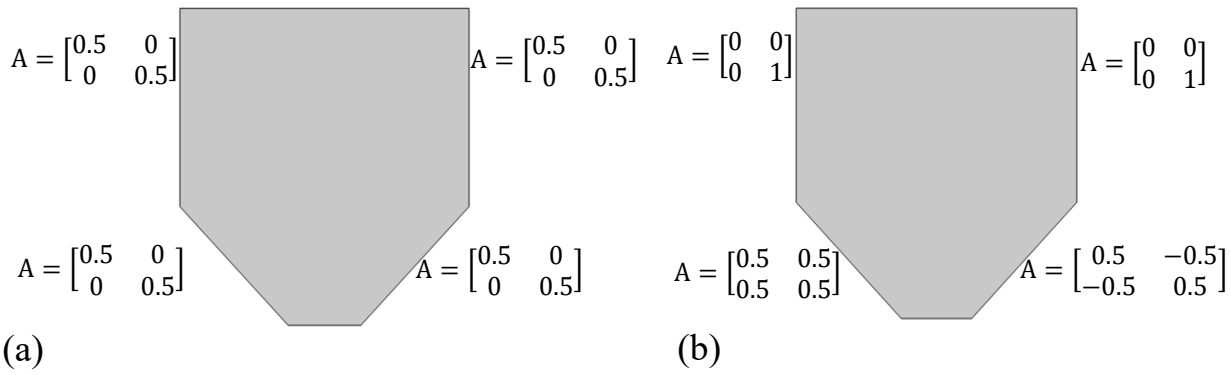

Figure 4.8. (a) Rugged walls, isotropic at all walls, (b) Flat walls, grains align with the boundaries' orientation

4.5. Findings and Analysis

In this section, the analysis delves into the impact of model parameters and boundary diffusion on the flow. Subsequently, the investigation proceeds to discern the reasons behind the flow changes attributed to grain orientation. Various boundary conditions have been taken into consideration to validate the functionality of the integrated model within the suite.

4.5.1. Velocity Profiles

The section includes the generation of 2-D velocity profiles to gain insight into how velocity and flow characteristics evolve from the hopper inlet to the outlet within the domain. This section specifically explores the influence of the model parameters λ and ψ, as well as the diffusion coefficient α, which signifies the effect of boundaries on grain orientation and the flow. The rheological model in equation (2.10) has an explicit dependency on the orientation, therefore, the velocity profile depends on the orientational field. Figures 4.9 and 4.10 depict velocity profiles for various diffusion coefficients and model parameters under the Rugged Boundary condition.

The initial results provide an overview of the flow inside the hopper under different scenarios in Figure 4.9. In Figure 4.9a, the Maximum Alignment Case of model parameters is implemented, allowing the grains to fully align with the flow which yields the least resistance for alignment. Figure 4.9b, on the other hand, features the Realistic Case of model parameters, to emphasize the influence of grains orientation on the flow. A comparison between these two figures reveals distinct responses. In the first case, where grains tend to well align with the flow, the velocity is higher compared to the second case where grains are less aligned. In the second scenario, with the model parameters as described, grains show less inclination to align fully with the flow, resulting in increased resistance to the flow, leading to a decrease in

velocity magnitude across the domain.

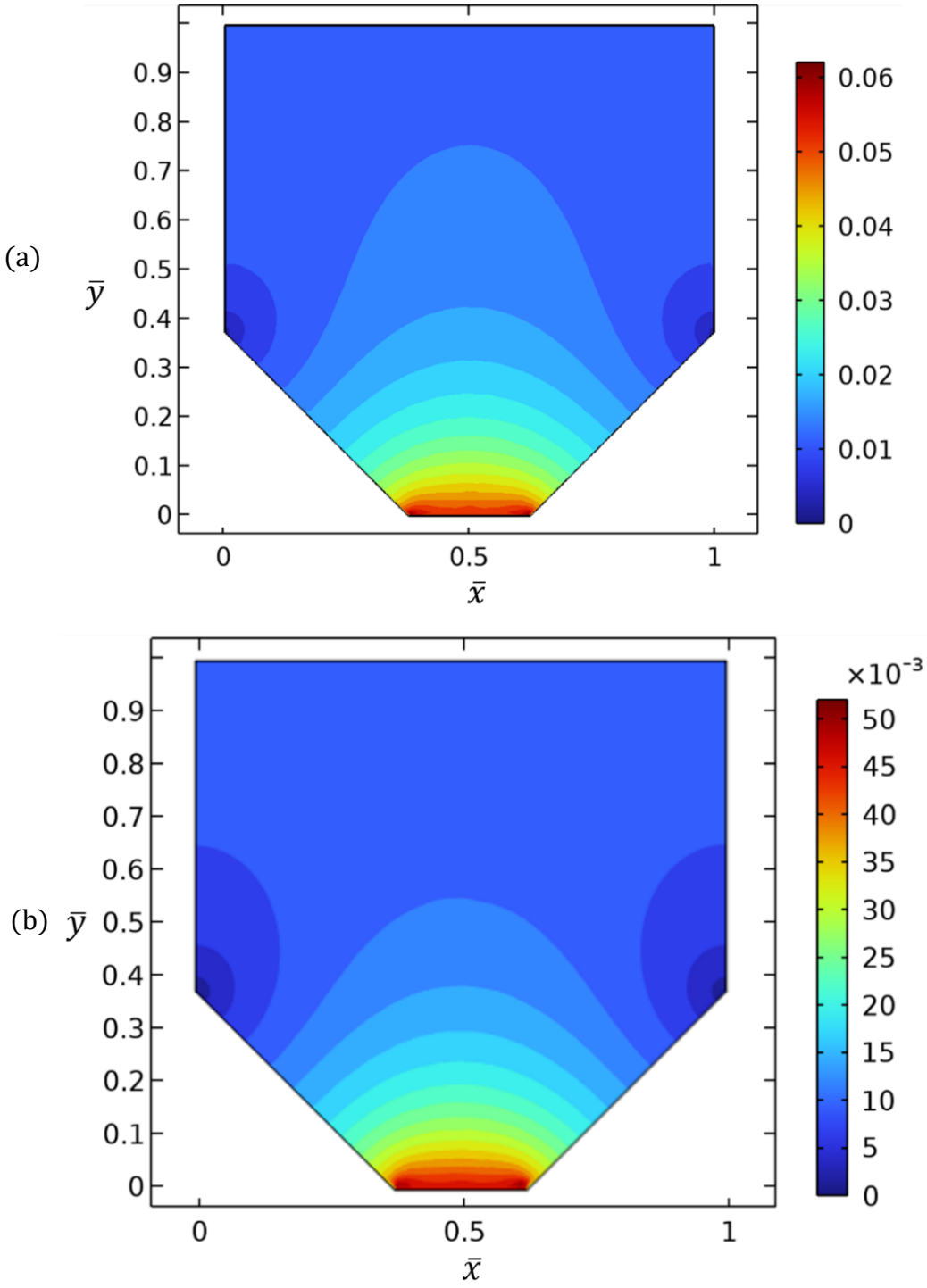

Figure 4.9. Velocity contours, (a) Realistic Case of model parameters and (b) Maximum Alignment Case of model parameters, while $\bar{\alpha} \approx 0$.

Furthermore, the stagnation zones within the hopper, where grains at the junction of

vertical and inclined walls and adjacent to the hopper walls remains at rest, are notably smaller in the first case. In the second case, due to a higher tendency of grains to flow, there is less congestion, and grains move more efficiently in the hopper. This demonstrates the significant impact of the tendency for alignment with the flow on the flow patterns and the velocity field within the domain.

To investigate the impact of boundary conditions on grains orientation, the diffusion coefficient, $\bar{\alpha}$, has been varied. In Figure 4.10, two velocity contours are depicted; Figure 4.10a where $\bar{\alpha} \approx 0$, signifying almost no diffusion in the flow, and Figure 4.10b where $\bar{\alpha} = 0.05$, indicating the presence of diffusion effect on grains orientation. These figures illustrate that as α increases, there is a slight alteration in the flow pattern. The stagnation zone expands, and the velocity within the entire hopper domain decreases. This effect is observed throughout the domain.

It is obvious that the velocity decreases as the diffusion coefficient increases, which is directly related to the rheological property that the flow resistance decreases as grains become more aligned with the flow. With increasing orientational diffusion the grains are more affected by the orientational boundary flux and, hence, less aligned.

These figures provide an initial visualization of the flow dynamics within the hopper, illustrating that the integration of specific model parameters and boundary conditions significantly impacts the velocity field and consequently induces meaningful alterations in the flow patterns across the domain. To gain a deeper understanding of the flow in various sections of the hopper, a sectional study is undertaken to elucidate the intricate details of the flow behavior.

It is obvious that the velocity decreases as the diffusion coefficient increases, which is directly related to the rheological property that the flow resistance decreases as grains become more aligned with the flow. With increasing orientational diffusion the grains are more affected by the orientational boundary flux and, hence, less

aligned. These figures provide an initial visualization of the flow dynamics within the hopper, illustrating that the integration of specific model parameters and boundary conditions significantly impacts the velocity field and consequently induces meaningful alterations in the flow patterns across the domain.

(a)

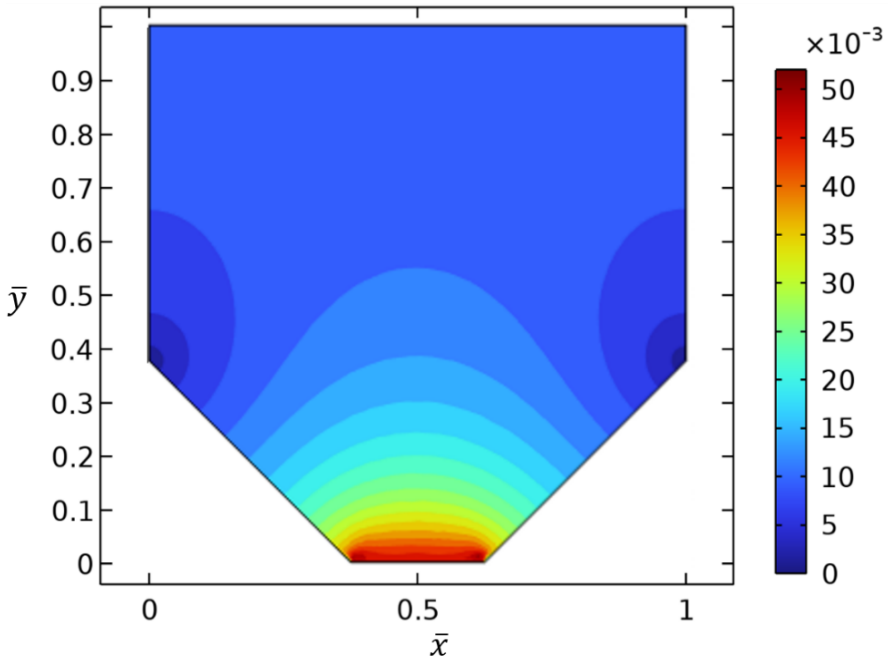

(b)

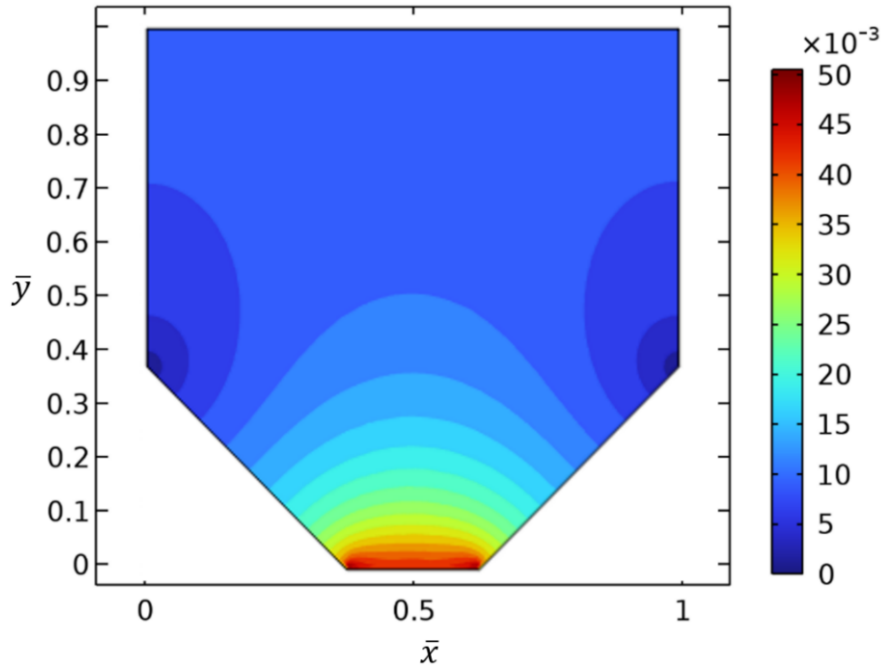

Figure 4.10. Velocity magnitude, a comparison between $(a)\ \bar{\alpha} \approx 0$, $(b)\ \bar{\alpha} = 0.05$, Maximum Alignment Case of model parameters

To gain a deeper understanding of the flow in various sections of the hopper, a sectional study is undertaken to elucidate the intricate details of the flow behavior.

In order to compare the flow behavior within the hopper, three heights of the hopper were chosen. As depicted in Figure 4.11, these sections include one in the upper part of the hopper with vertical walls, one in the transitional region connecting the vertical section to the hopper, and one in the lower part of the hopper, which encompasses the hopper with inclined walls. This approach allows for a comprehensive investigation of the flow evaluation, throughout the domain.

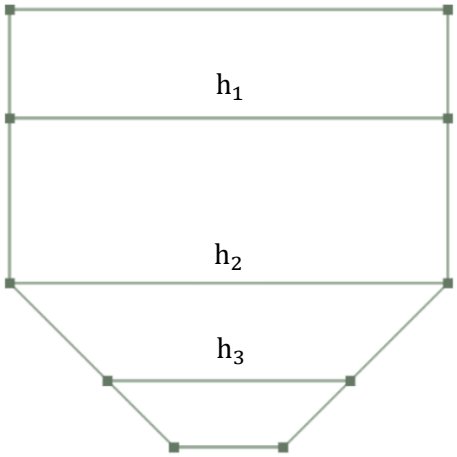

Figure 4.11. Selected sections for study in different heights of the hopper

To better understand the processes within the hopper, the subsequent figures illustrate the impact of the diffusion coefficient, $\bar{\alpha}$, on the flow inside the hopper. The figures are generated under two conditions: one in a very small value of diffusion flux, $\bar{\alpha} \approx 0$, and the other with diffusion effects, $\bar{\alpha} = 0.05, 0.5$. The choice of values for α was deliberate to clearly demonstrate its effect, as very small values do not significantly influence orientation, and very large values do not yield equilibrium orientation [24].

Figure 4.12 illustrates a comparison of velocity profiles under varying $\bar{\alpha}$ values, with the model parameters configured for the Maximum Alignment Case, to promote complete grain alignment and minimize flow resistance. These profiles have been

depicted for the three defined heights.

In Figure 4.12, It is evident from the profiles that in all sections, as $\bar{\alpha}$ increases, indicating an increased diffusion effect into the flow, the area with maximum velocity decreases. Furthermore, it is shown that velocity decreases as the diffusion coefficient increases, which is directly related to the effect of boundaries on the grains flow. As grains become more aligned with the flow, the flow resistance decreases. With increasing orientational diffusion, grains are more affected by the boundary, resulting in reduced alignment. As grains move toward the lower part of the hopper, the velocity increases, and the boundary layer of the flow expands, as observed from the velocity contours.

To compare the results of velocity profiles with different model parameters, the values of λ and ψ were changed to the Realistic Case, to observe the effect of grains orientation on the flow. The graphs in Figure 4.13 show 2D velocity profiles at the same predetermined hopper heights, each generated with different values of $\bar{\alpha}$.

As depicted in Figure 4.13 the impact of model parameters on the flow and velocity profiles is readily apparent. The velocity profiles reveal significant variations under identical simulation conditions due to the influence of model parameters.

The impact of model parameters remains consistent across different $\bar{\alpha}$ values. Where the Realistic Case of the model parameters is implemented, the velocity experiences a significant reduction at all heights, and the area with maximum velocity also shrinks. This reduction indicates less alignment with the flow and increased resistance against the flow. Irrespective of the grain's location within the domain, the implementation of the model parameters, as mentioned, significantly influences the flow pattern, and notably impacts the velocity magnitude.

a)h_1

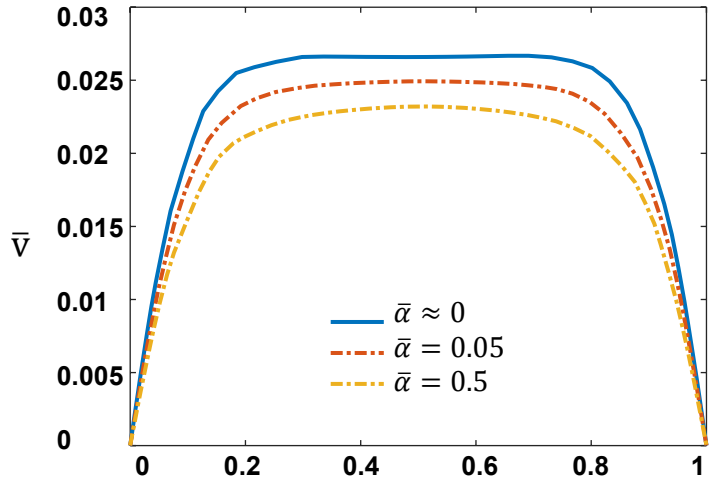

b)h_2

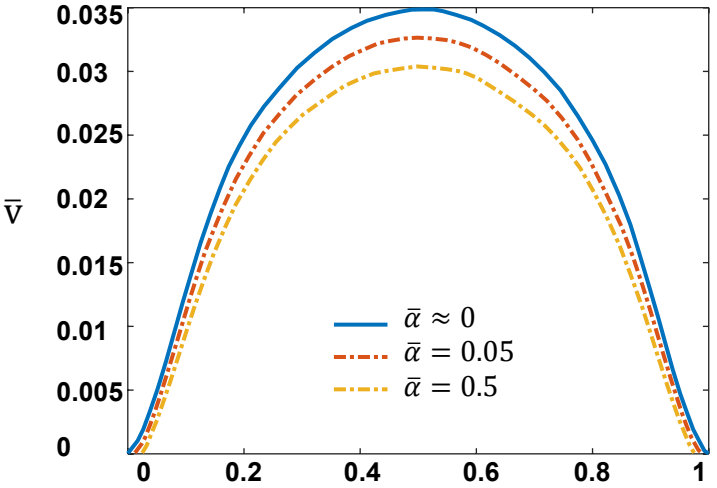

c)h_3

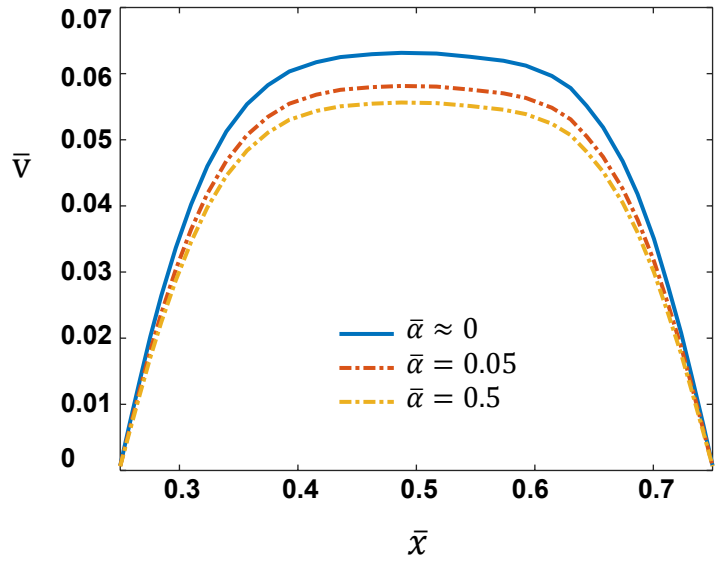

Figure 4.12. Velocity magnitude for three different diffusion coefficients, at three heights of the hopper

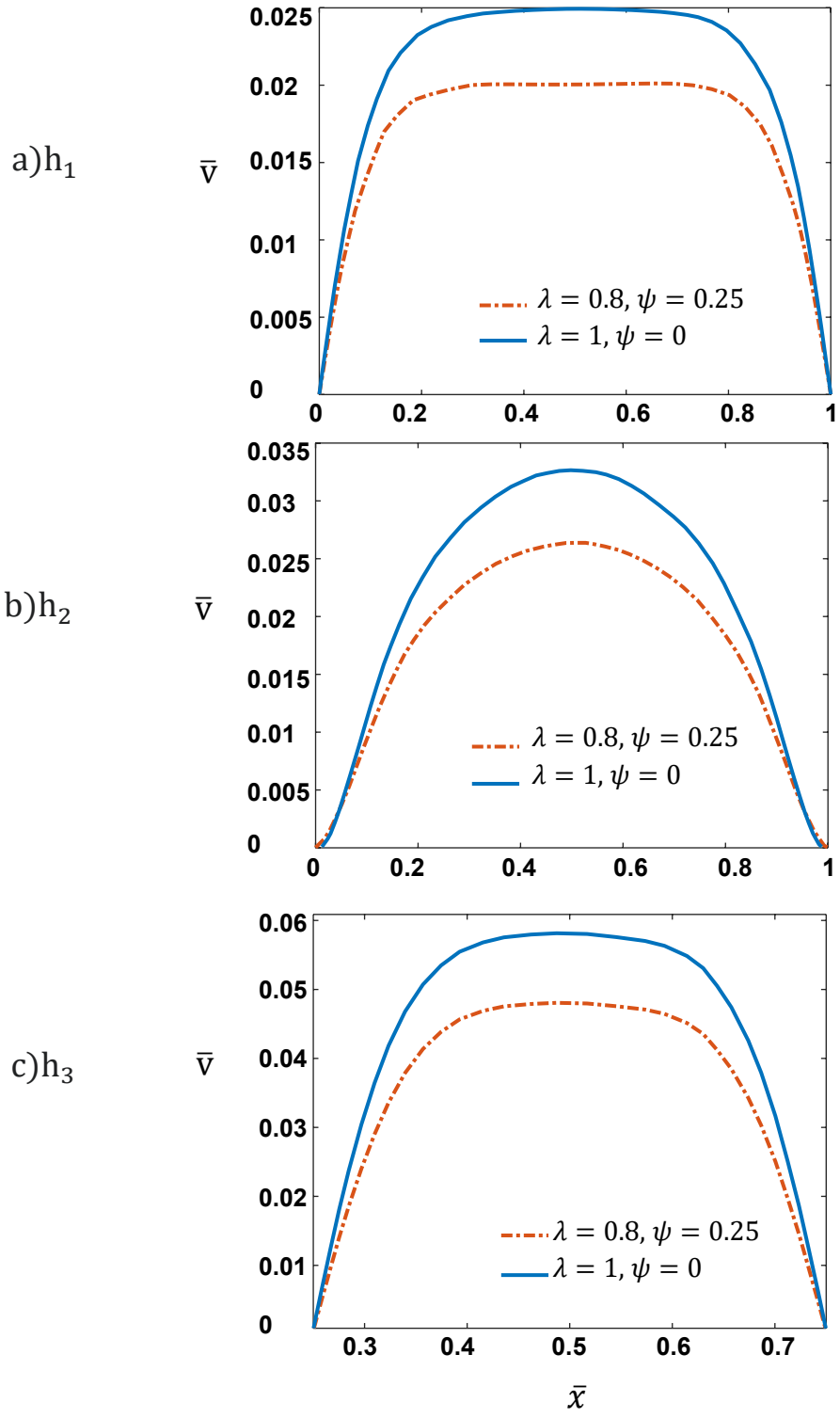

Figure 4.13. Velocity magnitude for two different sets of model parameters, in the presence of boundary effects, $\bar{\alpha} = 0.05$, at three heights of the hopper.

4.5.2. Orientational Angle and Ordering Factor

In the previous section, the effect of the model on the flow inside the hopper was studied and changes due to model parameters and diffusion effects were observed. To better understand the origins of these changes and how grains orientation and inertia rheology contribute to the velocity of the flow, further investigation is conducted.

To do this, the two measures of the orientational angle, θ, and the orientation ordering factor, ζ, as explained in section 3, are examined. The orientation matrix is obtained from the solution conducted by the simulation, and eigenvalues and eigenvectors are calculated. Subsequently, two-dimensional graphs depicting the variations in these two parameters are generated under different conditions.

This section contains figures illustrating the impact of the diffusion coefficient, on the orientational angle, θ, and the ordering factor, ζ, within the hopper at various heights. The heights of h_1 and h_3 have been selected to highlight the difference between the top section of the hopper with vertical walls and the bottom section with inclined walls. Additionally, to demonstrate the influence of model parameters on the flow, two situations with different tendencies for alignment are compared by varying the values of λ and ψ.

As mentioned previously, we examined two sets of boundary conditions correspond to the defined Flat and Rugged boundaries to investigate the model's performance under different scenarios and to facilitate a comparison between them. Consequently, the following results are categorized based on these two boundary conditions.

4.5.2.1. Rugged Boundary

This boundary condition is set to examine an isotropic condition for grains orientation at all walls.

In the first case a condition with the Maximum Alignment Case of the model parameters is investigated to promote maximum alignment of the grains with the flow while minimizing resistance to the flow. In Figure 4.14, the variations in the orientational angle, θ, and the ordering factor, ζ, in three different diffusion coefficients are depicted.

According to Figure 4.14a, at $h_1 = 0.3$ in the upper segment of the hopper, a clear distinction arises when comparing conditions with different diffusion coefficients, $\bar{\alpha}$, for both orientational angle, θ, and the ordering factor, ζ. This comparison vividly highlights the substantial influence of boundary effects on the orientational angle and the ordering factor. With $\bar{\alpha} \approx 0$, grains exhibit full alignment with the vertical flow in almost all areas of the section. However, as $\bar{\alpha}$ increases from zero, a boundary layer of grains effected by boundaries is obvious in the figures.

As $\bar{\alpha}$ increases further, the size of the boundary layer expands as the boundary flux diffuses further into the middle of the hopper. Grains located at a certain distance from the boundary reach a maximum angle, indicating a significant alignment with the vertical flow.

In reference to the ζ diagram, it commences at zero at the system's boundaries, symbolizing an isotropic state, and steadily rises to a maximum value. This upward trend indicates a substantial alignment of the grains with the vertical flow direction.

As evident from the depicted figure, the orientation of grains at the boundary interfaces showcases complete alignment with these boundaries. As one moves away from the boundaries, the grains gradually shift their alignment to match the direction of the flowing medium. Over a substantial portion of the section, the grains become fully oriented along the flow, indicating the transition from an isotropic condition at the boundaries to a well-organized alignment in the central region.

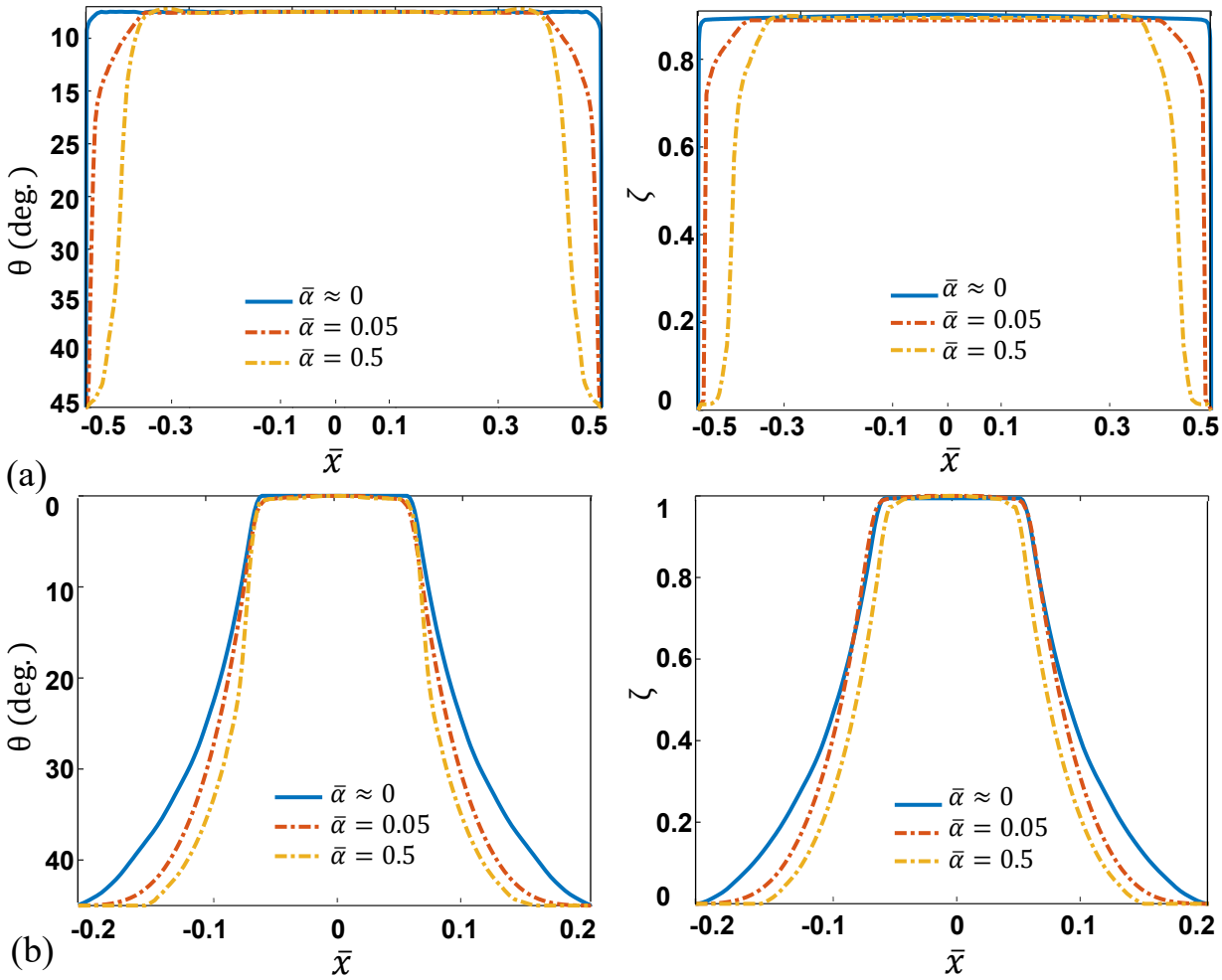

Figure 4.14. Variation of θ and ζ for three $\bar{\alpha}$ at two heights of the hopper (a) h_1, (b) h_3, Maximum Alignment Case of model parameters

With the introduction of boundary effects, denoted by the adjustment of the parameter $\bar{\alpha}$ from zero to 0.05, the influence of the boundaries becomes more pronounced. This effect is exemplified by the emergence of a distinct boundary layer between the hopper's walls and the flowing material, characterized by maximal orientation. As the value of $\bar{\alpha}$ increases, the size of this boundary layer expands due to diffusion, further influencing the orientation of the grains. Ultimately, the grains reach their peak orientation as grains move further away from the boundaries on both sides of the hopper. This transition in alignment underscores the impact of boundary conditions on the behavior and orientation of the grains within the hopper.

For a closer look at the flow in the lower part of the hopper, Figure 4.14b illustrates

a profile depicting the variation in grain angles and ordering factor at h_3. Due to the isotropic boundary conditions, the degree begins at 45 degrees at the boundaries and reaches the maximum angle of orientation in a part of the middle of the section. Evidently, in this part of the hopper, the area with full alignment of grains is smaller than in the upper part, as the inclined boundaries themselves influence the grains' orientation and prevent complete vertical alignment in this section. With an increase in $\bar{\alpha}$, the impact of boundaries becomes more pronounced, increasing the size of the boundary layers and hindering the grains from aligning with the flow due to the inclined angle of the boundaries. Furthermore, the orientation of grains has 0 degree of angle, representing the maximum alignment with the vertical downward flow and ordering factor shows 1, representing the highest mutual alignment between grains, particularly as the flow accelerates near the outlet of the hopper.

In the second case study, the values of model parameters are set to show the Realistic Case to emphasize the influence of grains orientation on the flow. As depicted in Figure 4.15, as expected, in both heights of the hopper, the region with full alignment decreases significantly. Even when $\bar{\alpha} \approx 0$ and there are no boundary condition effects on the grains, there is still a smaller region with the highest alignment with the vertical flow. This behavior intensifies as α increases, and due to the influence of boundaries, the grains near the wall align with the boundaries, while the region of full alignment diminishes accordingly. Similar behavior is observed in ζ.

It is important to highlight that as the model parameters decrease, reducing the tendency of grains to align, the grain angles and the orientation ordering factor also decrease in comparison to the previous results.

In the upper part of the hopper the grains angle reaches a maximum of less than 10 degrees, and the orientation reaches a maximum of less than 0.8, which both are less than the correspondence values for the previous case with the Maximum Alignment

Case of model parameters. In the lower part of the hopper, this misalignment is more pronounced, particularly near the walls. However, as the flow accelerates toward the outlet, the maximum grains angle and the ordering factor increase to their peak values of 0 degrees and 1, respectively.

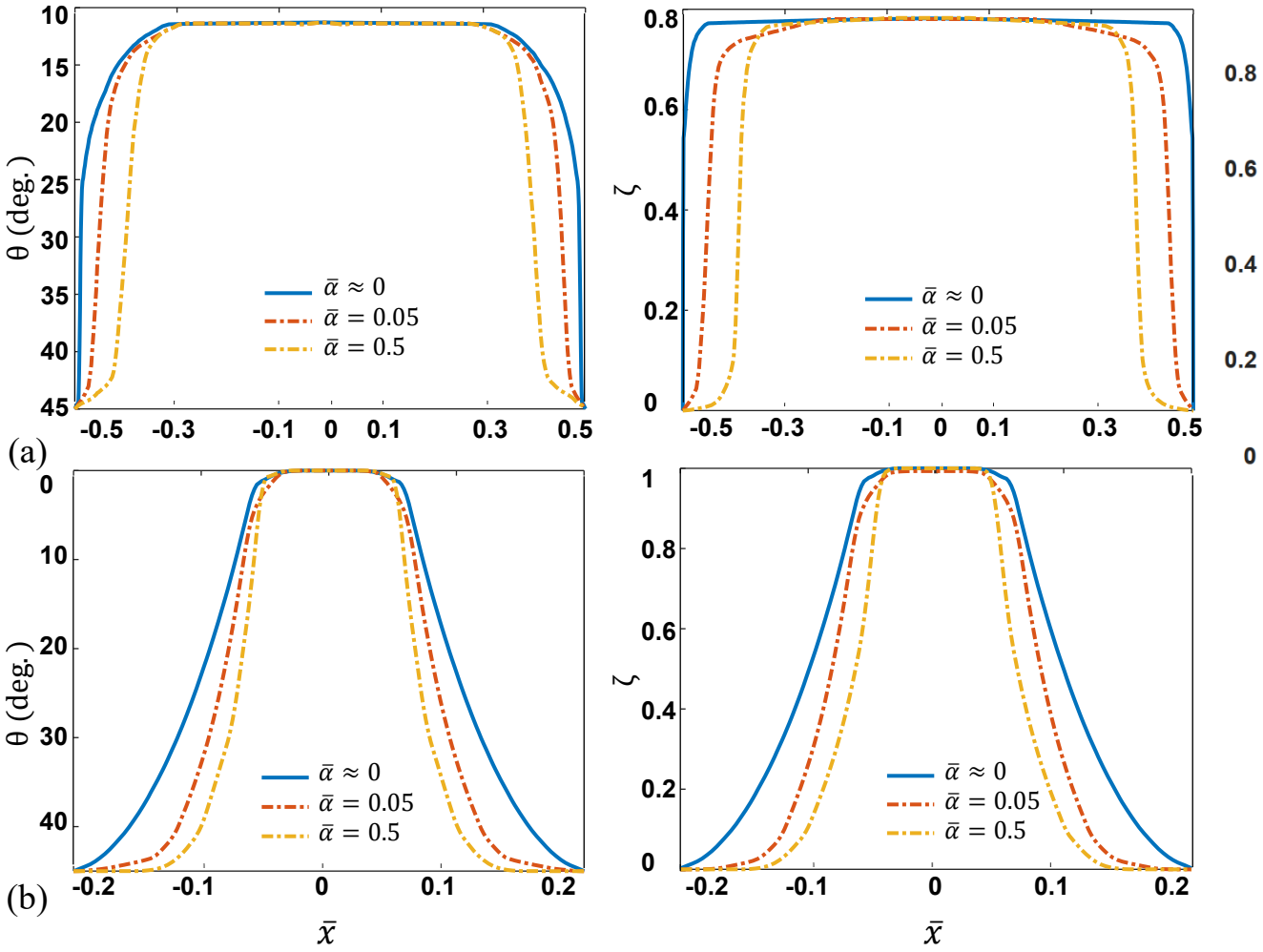

Figure 4.15. Variation of θ and ζ for three $\bar{\alpha}$, in two heights of the hopper (a) h_1, (b) h_3, Realistic Case of model parameters

These results are qualitatively in good agreement with the findings obtained in [24], both in terms of the variation patterns and the impact of boundary conditions and model parameters on the flow of granular materials.

4.5.2.2. Flat Boundary

In the last part of this section, a Flat boundary is examined, where the orientation of

grains in contact with the boundary is fully aligned with the boundary orientation to assess the effectiveness of the model under a different boundary condition and compare with the results for the previous case.

To this end, three different values of $\bar{\alpha}$ and two different sets of λ and ψ (the same as those examined in the previous section with Rugged boundary conditions) are studied to understand how the model performs when subjected to new boundary conditions. It is worth noting that as the sample hopper has inclined walls in the lower part at a 45-degree angle, the results for the lower part are the same as in the previous section. Therefore, the following figures are generated at $\mathrm{h}_1 = 0.3$, located at the upper part of the hopper.

In Figure 4.16a, the variation of the orientational angle, θ, under three different diffusion coefficients presented. The model parameters in this case are according to the Realistic Case, designed to have a significant effect on grains orientations. As seen in the figure, the angle of grains starts at 0 degrees due to the boundary conditions and experiences a sharp decrease, reflecting the initial isotropic orientation of grains. However, this angle gradually increases due to the flow, reaching its maximum alignment with the vertical flow. As $\bar{\alpha}$ increases, the influence of boundaries on grains orientation becomes more pronounced, resulting in a thicker boundary layer.

In Figure 4.16b, the variation of the ordering factor, ζ, for different diffusion coefficient is depicted. The variation pattern is similar to the orientational angle variation, showing the impact of boundary conditions on the level of mutual alignment of grains.

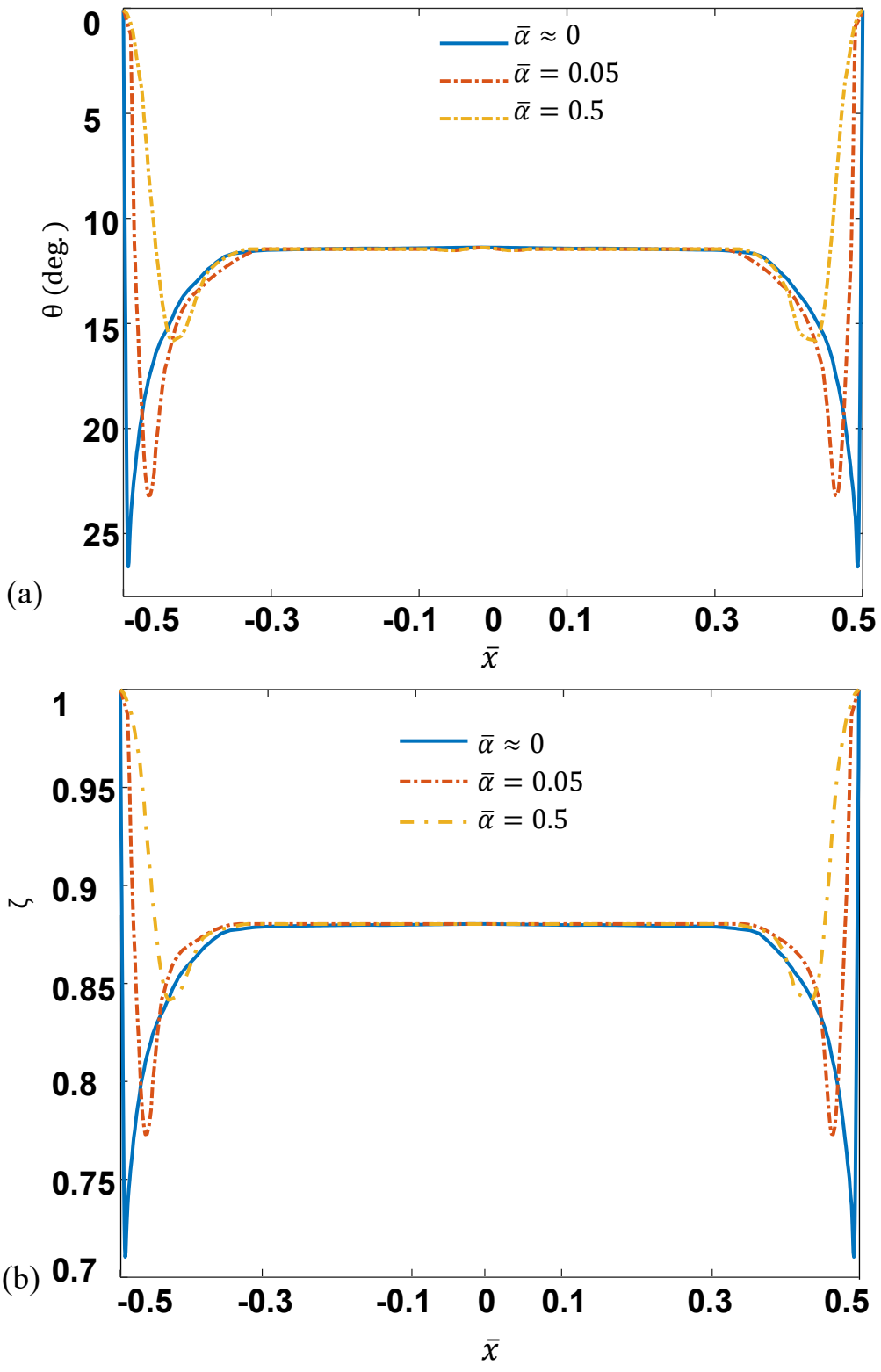

Figure 4.16. Variation of θ and ζ for three different diffusion coefficients, at $h_1 = 0.3$, Realistic Case of model parameters

In the second case, as depicted in Figure 4.17, the model parameters are set to represent the Maximum Alignment Case to examine a situation with the highest tendency for alignment and the least resistance against flow due to grains misalignment.

As is demonstrated in Figure 4.17, in this case, the area with maximum alignment with the vertical flow increases significantly. The maximum orientational angle also aligns with previous findings under Rugged boundary condition. In this scenario, the grains along the walls initially have an angle of 0 degrees due to the boundary conditions. After a sharp decrease, attributed to the initial isotropic state, the angle increases until it reaches the maximum value for the orientation angle, which is evidently greater than in the case of Figure 4.16a. Given the stronger tendency for alignment in this case, the effect of boundary conditions is less prominent, and the boundary layer is thinner than in the previous case of Figure 4.16a. Once again, as $\bar{\alpha}$ increases, the impact of boundary conditions and the diffusion flux becomes more evident, causing the grains to align with the vertical flow across a wider region of the selected section. The same behavior is evident in Figure 4.17b, leading to a similar interpretation for comparing the ordering factor between the two sets of model parameters.

All the presented examinations and the resulting data clearly demonstrate the robust capabilities of the model. The accuracy of the simulations has been verified through a comparison with experimental data and examined with different geometries and boundary conditions, affirming its reliability. These positive outcomes underscore the feasibility of extending the model to more intricate studies and applications, showcasing its adaptability to complex scenarios.

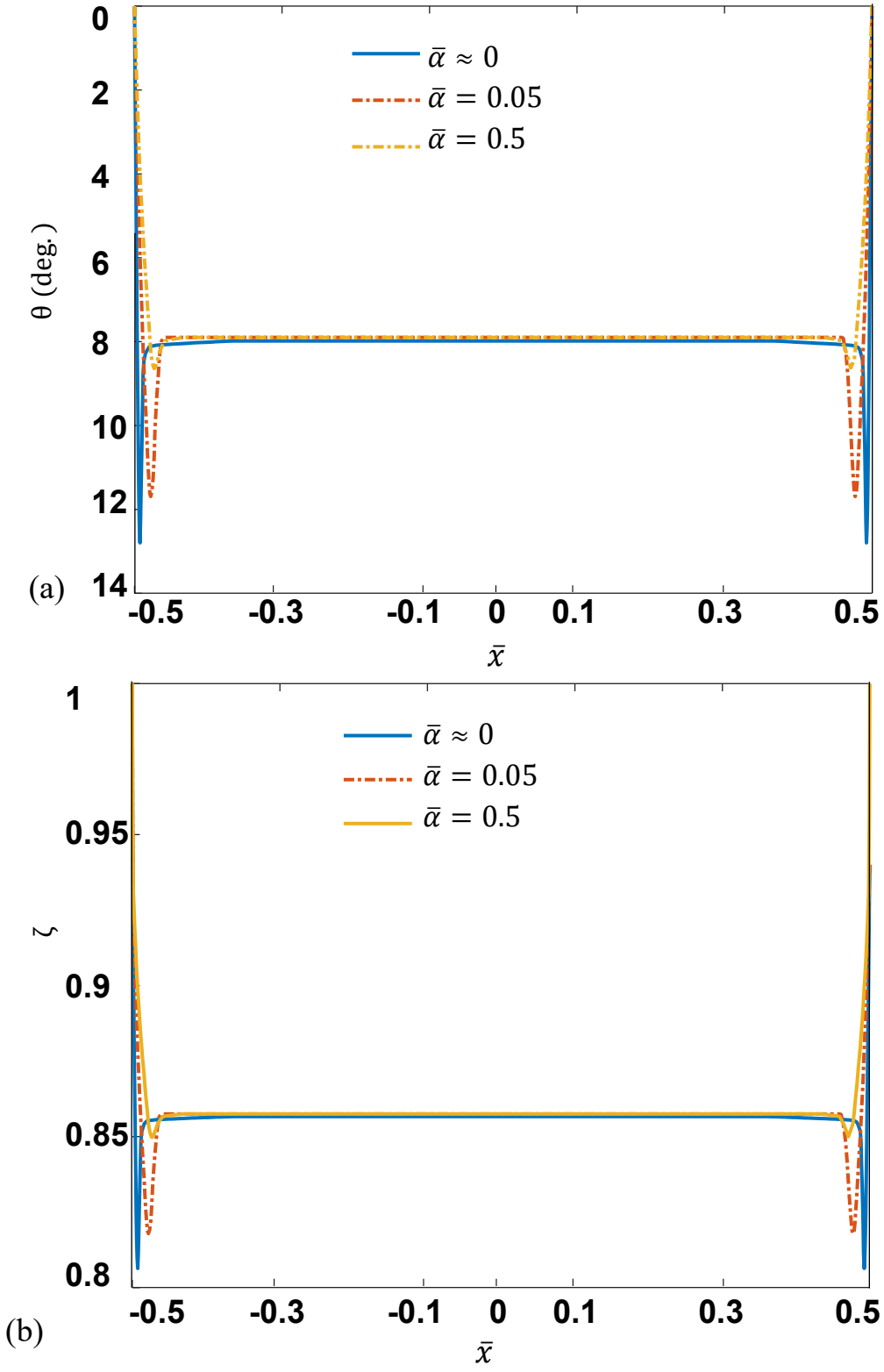

Figure 4.17. Variation of θ and ζ for three different diffusion coefficients, at $h_1 = 0.3$, Maximum Alignment Case of model parameters

Chapter 5

5. Conclusions and Future Works

This chapter offers a concise summary of the research conducted, highlighting the key findings. Additionally, it identifies the primary enhancements achieved in this study and provides suggestions for potential future research endeavors.

In this study, we have implemented and numerically solved an existing developed model to simulate the behavior of non-spherical grains within a two-dimensional hopper using the versatile COMSOL Multiphysics® suite. Our study extensively probed the influence of model parameters and boundary conditions on grains orientation and velocity. A good agreement with an experimental study in obtaining the velocity and orientation field of different types of grains was achieved. Moving forward to more complex geometry and more practical conditions, notably, our findings were qualitatively in good alignment with the results of a previous study, which employed a similar approach to implement the same model in a simpler geometric setting.

One of the primary challenges encountered in this study pertained to rendering the model equations compatible with the FEA suite and implementing the existing modules within the suite to incorporate both the evolution law equation and the inertia rheology equation. By selecting appropriate values for the coefficients and identifying suitable terms in COMSOL Multiphysics, the integration was done properly, resulting in an accurate simulation. The primary motivation for this study was to lay the groundwork for the implementation of complex problems involving non-spherical granular materials using a FEA simulation suite. We aimed to leverage the capabilities of this suite for seamless integration with various Computer-Aided Design and Analysis tools to facilitate investigations across a wide spectrum of geometries and conditions.

5.1. Concluding Remarks

The following observations and improvements have been identified in this study, which differ from previous studies implementing the same model:

- We implemented the developed models for orientation and stress as partial differential equations with derivatives in both temporal and spatial variables. This allowed us to obtain solutions for both velocity and orientation fields. We also examined the impact of boundaries and geometry on both the velocity and orientation fields in a hopper. This is a notable improvement over previous studies in a hopper using the same model, which were limited to solving an ordinary differential equation with a focus only on the orientation equation, neglecting geometry and boundary effects.
- In COMSOL Multiphysics, there is no physics module designed to comprehend orientation. To address this, we manually created a new module that integrates the governing equations of orientation and the balance of linear momentum into the suite, along with defining new boundary conditions within the suite.
- This implementation of the new physics module has the potential to serve as a pilot for future studies, allowing for easy modification of geometry and boundary conditions. It also provides flexibility for those looking to further develop the model. Without this suite implementation, solving these equations through MATLAB coding is feasible only for very simple geometries where studying the flow in 3D geometries or complex shapes is significantly difficult and challenging. Moreover, this physics module can be seamlessly coupled with other predefined physics in COMSOL Multiphysics, such as electromagnetic or chemical physics, for research in various fields related to granular materials.

There were also some limitations in this study as follows:

- The selected settings in the suite for this study, including the timesteps, type of solver, and type of coupling, and their respective options, may not necessarily be

suitable for simulating all geometries and conditions. Adjustments should be made accordingly. In general, for large scale problems, such as 3D and complex domains with large dimensions, other coupling models and solvers like segregated coupling model should be examined as fully coupled solver has a high computational cost. Also, different types of meshes and suitable time steps should be considered for optimizing the computational cost and accuracy of simulation.

- Although comparison with experiments on flows in a hopper has shown that the model provides a realistic description of the orientational field, more experimental data on the grains' orientation near the boundary surface is required to further evaluate the accuracy of the model in these regions.

5.2. Future Works

As previously emphasized, further experimental data are essential to comprehensively evaluate the model's accuracy. To this end, the model opens the door to an array of possibilities for examining granular material flow within hoppers, encompassing a wide variety of geometries and conditions. Potential directions for future research include:

- Geometry optimization: This simulation suite can be a valuable tool for enhancing the design of hoppers with internal components, aiming to address congestion issues that commonly impact industrial processes. By simulating different geometrical configurations and examining their impact on granular material flow, more efficient and effective designs can be developed.
- Boundary Conditions Exploration: Diverse boundary conditions can be implemented to investigate their influence on granular material flow. For instance, the introduction of wavy boundary conditions can simulate the effects of mechanical vibrators installed on hopper walls to facilitate material flow. Such studies can provide insights into optimizing boundary conditions for specific

industrial applications.

- 3D hopper modeling: While this study focused on a 2D hopper, future research can extend into three-dimensional hopper modeling. A 3D model would provide a more realistic representation of granular material behavior inside hoppers, yielding more accurate results and a deeper understanding of the grains' flow. For that, the same approach can be followed to integrate the developed model for 3D.
- Enhancing hopper modeling capabilities: Advanced CAD Integration allows the suite to import complex geometries through CAD suite linkage, facilitating the modeling of intricate hopper structures. Furthermore, the ability to export data for analysis with other suite tools enhances post-processing capabilities and research outcome robustness.

Bibliography

[1] Duran, J. (1999). Sands, Powders, and Grains: An Introduction to the Physics of Granular Materials (A. Reisinger, Trans.). Springer-Verlag New York, Inc.

[2] Rhodes, M. (Ed.). (1997). Principles of Powder Technology. John Wiley and Sons.

[3] Duran, J. (2012). Sands, Powders, and Grains: An Introduction to the Physics of Granular Materials

[4] Jaeger, H. M., Nagel, S. R., and Behringer, R. P. (1996). Granular Solids, Liquids, and Gases. Rev. Mod. Phys, 68(10), 1259-1273.

[5] Brennen, C. E. (2005). Granular Flows. Cambridge University Press.

[6] Forterre, Y., and Pouliquen, O. (2008). Flows of Dense Granular Media. Annu. Rev. Fluid Mech., 40, 1-24.

[7] Shook, C. A., and Roco, M. C. (1991). Slurry Flow: Principles and Practice (2nd ed.). Butterworth-Heinemann.

[8] Nortje, D. (2002). The Anti-Dynamic Tube in Mass Flow Hoppers (PhD thesis). The University of Western Australia, Department of Civil and Resource Engineering.

[9] Harrison, D. (1974). Fluidization. Science Progress (1933-), 61(242), 191–217.

[10] Brennen, C. E. (2005). Fundamentals of Multiphase Flows. Cambridge University Press.

[11] Iverson, R. M., Reid, M. E., and Lahusen, R. (1997). Debris-Flow Mobilization from Landslides. Annual Review of Earth and Planetary Sciences, 25(1), 85-138.

[12] Hutter, K., Wang, Y., and Pudasaini, S. P. (2005). The Savage-Hutter

Avalanche Model: How Far Can It Be Pushed? Philosophical Transactions: Mathematical, Physical and Engineering Sciences, 363(1832), 1507–1528.

[13] Hughes, F., and Madabhushi, S. (2019). Liquefaction-Induced Displacement and Rotation of Structures with Wide Basements. https://doi.org/10.17863/CAM.36393.

[14] Nedderman, R. M. (1992). Statics and Kinematics of Granular Materials. Cambridge University Press.

[15] Goldhirsch, I. (2003). Rapid Granular Flows. Annual Review of Fluid Mechanics, 35(1), 267-293.

[16] Johnson, P. C., and Jackson, R. (1987). Frictional–Collisional Constitutive Relations for Granular Materials, with Application to Plane Shearing. Journal of Fluid Mechanics, 176, 67-93.

[17] Tang, J., and Behringer, R. P. (2016). Orientation, Flow, and Clogging in a Two-Dimensional Hopper: Ellipses vs. Disks. EPL (Europhysics Letters), 114(3), 34002.

[18] Azéma, E., Preechawuttipong, I., and Radjai, F. (2016). Binary Mixtures of Disks and Elongated Particles: Texture and Mechanical Properties. Physical Review E, 94(4), 042901.

[19] Börzsönyi, T., Somfai, E., Szabo, B., Wegner, S., Mier, P., Rose, G., and Stannarius, R. (2016). Packing, Alignment, and Flow of Shape-Anisotropic Grains in a 3D Hopper Experiment. New Journal of Physics, 18(9), 093017.

[20] Wegner, S., Stannarius, R., Boese, A., Rose, G., Szabo, B., Somfai, E., and Börzsönyi, T. (2014). Effects of Grain Shape on Packing and Dilatancy of Sheared Granular Materials. Soft Matter, 10(28), 5157-5167.

[21] Nadler, B., Guillard, F., and Einav, I. (2018). Kinematic Model of Transient

Shape-Induced Anisotropy in Dense Granular Flow. Physical Review Letters, 120(19), 198003.

[22] Nadler, B. (2021). Anisotropic Inertia Rheology of Ellipsoidal Grains. Granular Matter, 23(1), 14.

[23] Amereh, M., and Nadler, B. (2022). A Generalized Model for Dense Axisymmetric Grains Flow with Orientational Diffusion. Journal of Fluid Mechanics, 936, A40.

[24] Ashour, A., Wegner, S., Trittel, T., Börzsönyi, T., and Stannarius, R. (2017). Outflow and Clogging of Shape-Anisotropic Grains in Hoppers with Small Apertures. Soft Matter, 13(2), 402-414.

[25] Börzsönyi, T., and Stannarius, R. (2013). Granular Materials Composed of Shape-Anisotropic Grains. Soft Matter, 9(31), 7401-7418.

[26] Yong, H. W. (1990). Static and Dynamic Analysis of Flow of Bulk Materials through Hoppers. University of Wollongong Thesis Collection

[27] Schulze, D. (2007). Powders and Bulk Solids – Behavior, Characterization, Storage, and Flow. Springer Berlin.

[28] Guillard, F., Marks, B., and Einav, I. (2017). Dynamic X-ray Radiography Reveals particle size and shape orientation fields during granular flow. Science Reports.

[29] Zuriguel, I., Garcimartín, A., Maza, D., Pugnaloni, L. A., & Pastor, J. M. (2005). Jamming during the discharge of granular matter from a hopper. Physical Review E - Statistical, Nonlinear, and Soft Matter Physics, 71(5).

[30] Eman, H., Newson, T., and Ahmed, A. (2020). The Dynamics of Granular Flow in Hopper Hoppers. Geotechnical Research Centre, University of Western Ontario.

[31] Jop, P., Forterre, Y., and Pouliquen, O. (2006). A Constitutive Law for Dense Granular Flows. Nature, 441(7094), 727-730

[32] COMSOL Multiphysics® v. 6.0, www.comsol.com, COMSOL AB, Stockholm, Sweden.

[33] COMSOL AB. (2019). COMSOL Multiphysics®. COMSOL Reference Manual. Retrieved from https://www.doc.comsol.com.

[34] Jin, W., O'Hern, C. S., Radin, C., Shattuck, M. D., & Swinney, H. L. (2020). Homogeneous Crystallization in Cyclically Sheared Frictionless Grains. Phys. Rev. Lett. 125, 258003. https://doi.org/10.1103/PhysRevLett.125.258003

[35] Hidalgo, R. C., Szabó, B., Gillearot, K., Börzsönyi, T., and Weinhart, T. (2018). Rheological Response of Nonspherical Granular Flows Down an Incline. Phys. Rev. Fluids, 3, 074301

[36] Leading Engineering Application Providers (LEAP). (2012). Tips and Tricks. Retrieved from www.computationalfluiddynamics.com.au.